

LUT UNIVERSITY
LUT School of Energy Systems
LUT Mechanical Engineering

Jaakko Simonen

**EFFECT OF WELDING BOUNDARY CONDITIONS ON THE RESIDUAL
STRESSES AND THE FATIGUE STRENGTH OF A TRANSVERSAL
ACCESSORY JOINT**

Examiners: Professor Timo Björk
D.Sc. (Tech.) Tuomas Skriko
M.Sc. (Tech.) Antti Ahola

TIIVISTELMÄ

LUT-Yliopisto
LUT School of Energy Systems
LUT Kone

Jaakko Simonen

Hitsausreunaehtojen vaikutus poikittaisen varusteluliitoksen jäännösjännityksiin ja väsymiskestävyyteen

Diplomityö

2020

73 sivua, 37 kuvaa, 13 taulukkoa ja 3 liitettä

Tarkastajat: Professori Timo Björk
Tkt Tuomas Skriko
DI Antti Ahola

Hakusanat: väsyminen, jäännösjännitys, teräs, hitsaus, röntgendiffraktio

Ultralujat teräkset (UHSS) ja niiden väsymisominaisuudet ovat alati tärkeämpiä tutkimusaloja nykyaikaisen teollisuuden sekä erityisesti loppuasiakkaiden vaatiessa kevyitä ja pitkäkestoisia rakenteita. Näissä korkean myötölujuuden omaavissa materiaaleissa myös hitsauksen aiheuttamat jäännösjännitykset ovat tyypillisesti korkeita. Tämän vuoksi hitsausjäännösjännitysten tutkiminen sekä niiden vaikutuksen arvioiminen ultralujien terästen hitsausliitosten väsymislujuuteen ovat muodostuneet erityisen huomionarvoisiksi tutkimuskohteiksi.

Tässä työssä tarkastellaan hitsauksen aikaisten reunaehtojen vaikutusta sekä UHSS-liitoksen jäännösjännityksiin että sen väsymiskestävyyteen. Lisäksi tehdään ehdotelma hitsausjäännösjännityskomponenttien luokittelusta. Luokittelu perustuu siihen, millä tavalla jäännösjännitysten tasapainotilanne rakenteessa muodostuu. Käytännön laboratoriokokeissa hitsattiin poikittaisriipa pienahitsillä peruslevyyn kolmella erilaisella reunaehdolla: vapaalla, jäykällä ja puolijäykällä tuennalla. Pinnan jäännösjännitysprofiilit hitsin läheisyydessä mitattiin röntgendiffraktio-menetelmällä, ja väsymiskestävyydet määritettiin väsytysokeilla, joissa kuorma oli vakioamplitudinen ja yksiakselialinen. Tutkittava perusmateriaali oli ultraluja teräs SSAB Strenx 1100 Plus.

Tulosten perusteella voidaan todeta, että hitsauksen aikainen jäykkä reunaehto tuottaa oleellisesti suurempia vetojäännösjännityksiä verrattuna muihin reunaehdotapauksiin, joissa hitsausmuodonmuutokset saivat tapahtua vapaammin. Väsymiskestoikä lyhenee, kun hitsausreunaehdon jäykkyyttä kasvatetaan eli muodonmuutosten syntymistä estetään.

ABSTRACT

LUT University
LUT School of Energy Systems
LUT Mechanical Engineering

Jaakko Simonen

Effect of Welding Boundary Conditions on the Residual Stresses and the Fatigue Strength of a Transversal Accessory Joint

Master's Thesis

2020

73 pages, 37 figures, 13 tables and 3 appendices

Examiners: Professor Timo Björk
D.Sc. (Tech.) Tuomas Skriko
M.Sc. (Tech.) Antti Ahola

Keywords: fatigue, residual stress, steel, welding, X-ray diffraction

Ultra-high strength steels (UHSS) and their fatigue properties are study fields of growing importance, as the modern industry and especially the end customers demand light-weight, long-lasting structures. In these materials of high yield strength, the welding-induced residual stresses are typically also high. Therefore, the study of welding residual stresses and the evaluation of their effect on the fatigue strength of UHSS joints have become research topics of significant value.

In this work, the influence of welding boundary conditions on both the residual stresses and the fatigue strength of a UHSS joint are studied. In addition, a proposal is made for the categorization of the welding residual stress components, according to how the equilibrium condition is formed in the structure. In experimental laboratory tests, a transverse attachment was fillet-welded on a baseplate under three different restraint conditions: free, fixed and semi-rigid support. The surface residual stress profiles in the vicinity of the weld were measured with X-ray diffractometry, and fatigue tests with constant amplitude uniaxial loading were made to determine the fatigue strengths. The studied base material was SSAB Strenx 1100 Plus.

The results indicate that the rigid boundary condition during welding creates substantially higher tensile residual stresses compared to the other boundary conditions, where the welding deformations were allowed to occur more freely. The fatigue life decreases alongside with the increase of the rigidity of the welding boundary condition.

ACKNOWLEDGEMENTS

“Bless the Lord, all his works in all places of his dominion”. Ps. 103:21.

In addition, I want to thank my supervisors Timo Björk, Tuomas Skriko and Antti Ahola for sharing their expertise with me for the benefit of this thesis. It has been a pleasure to work with real professionals. I also thank the employees of the Laboratory of Steel Structures for arranging and performing the experimental tests. Our collaboration has been a rich learning experience. Likewise, I want to thank all staff members from other laboratories who have contributed to the completion of this work. My warm thanks go to all my friends who have remembered me in their prayers.

Finally, I want to thank you, my beloved Iris, for your patience, longsuffering, and love. For eight years to date, you have given the joy and purpose to my life. I am perfectly aware that without your support, this work would never have been even started, let alone finished. And as we know, the heaviest and most important work is not done in laboratories or research institutes, but at those homes where loving mothers bring up their youth in the shelter of the Almighty.

TABLE OF CONTENTS

TIIVISTELMÄ

ABSTRACT

ACKNOWLEDGEMENTS

TABLE OF CONTENTS

LIST OF SYMBOLS AND ABBREVIATIONS

1	INTRODUCTION	10
	1.1 Research problem	11
	1.2 Aims.....	12
	1.3 Research questions.....	12
	1.4 Methods	12
	1.5 Delimitations.....	13
2	FATIGUE OF WELDED JOINTS	14
	2.1 Fatigue phenomenon.....	14
	2.2 Crack nucleation	14
	2.3 Crack propagation.....	15
	2.4 The impact of welding on fatigue strength	16
	2.5 The impact of mean stress on fatigue strength	17
	2.6 Fatigue evaluation methods	17
	2.6.1 Nominal stress method.....	17
	2.6.2 4R method.....	18
3	WELDING RESIDUAL STRESS	20
	3.1 Residual stress.....	20
	3.2 Tensile welding residual stresses due to thermal contraction.....	21
	3.3 Welding residual stresses due to phase transformation	22
	3.4 Impact of residual stress on fatigue strength	23
	3.5 Measurement of welding residual stress	23
	3.5.1 X-ray diffraction measurement of welding residual stress	24
	3.5.2 Neutron diffraction measurement of welding residual stress.....	25
	3.6 Recent research into residual stress effects on fatigue	26
4	RESIDUAL STRESS CATEGORIZATION	30

4.1	Existing categorization of macroscopic residual stresses	30
4.2	New proposal for the categorization of macroscopic residual stresses	31
4.2.1	Primary residual stresses	32
4.2.2	Secondary residual stresses	33
4.2.3	Tertiary residual stresses	35
5	MATERIALS AND METHODS	37
5.1	Experimental testing	37
5.1.1	Batch 1: Unconstrained.....	38
5.1.2	Batch 2: Fixed	39
5.1.3	Batch 3: Semi-rigid	40
5.1.4	Loads	41
5.1.5	Materials and welding parameters	43
5.1.6	Post weld treatment	44
5.2	Numerical analysis.....	45
5.2.1	Secondary bending.....	45
5.2.2	Evaluation with nominal stress method	47
5.2.3	Evaluation with 4R method	48
5.2.4	FEA	49
6	RESULTS	52
6.1	Temperature history	52
6.2	Welding deformations.....	53
6.3	Residual stresses	54
6.4	Fatigue lives	58
6.5	S-N curves.....	62
7	DISCUSSION	65
7.1	Analysis of results.....	65
7.2	Test arrangement shortcomings	66
8	CONCLUSIONS	68
	REFERENCES	70
	APPENDIX	73
	Appendix I: Cross section of batch 3 specimen.	
	Appendix II: Vickers hardness distributions of weld area.	
	Appendix III: Strain alterations in batch 3 specimens during HFMI treatment.	

LIST OF SYMBOLS AND ABBREVIATIONS

a	Lattice parameter [-]
b	Plate width [mm]
C	Paris constant [mm/(cycle·(MPa·m ^{0.5}) ^m)]
C_{char}	Characteristic fatigue capacity [-]
C_{mean}	Mean fatigue capacity [-]
C_{ref}	Reference fatigue capacity [-]
D	Cross section area [mm ²]
da/dN	Crack growth rate [mm/cycle]
F_i	Pre-load force [N]
$F_{support}$	Support reaction force [N]
K	Stress intensity factor [MPa·mm ^{0.5}]
h, k, l	Miller indices [-]
$k_{m,calc}$	Calculated stress magnification factor [-]
$k_{m,cov}$	Stress magnification factor already covered in the design curve [-]
$k_{m,eff}$	Effective stress magnification factor [-]
$k_{t,b}$	Bending notch stress factor [-]
$k_{t,m}$	Membrane notch stress factor [-]
L	Clamping length [mm]
m	Slope of S-N curve, Paris exponent [-]
m_{ref}	Slope of reference S-N curve [-]
$M_{support}$	Support reaction moment [Nmm]
n	Order of reflection [-]
N_f	Final fatigue life, number of cycles [-]
P_s	Survival probability [%]
R	Stress ratio [-]
R_m	Ultimate strength [MPa]
$R_{p0.2}$	Proof strength [MPa]
S	Applied nominal membrane stress [MPa]
r_{true}	Actual toe radius [mm]

t	Plate thickness [mm]
$t_{8/5}$	Cooling time from 800 °C to 500 °C [s]
y_m	Flange mid-plane distance from neutral axis [mm]
α	Wavelength [nm]
α_d	Distortion angle [°]
ΔK	Stress intensity range [MPa·mm ^{0.5}]
ΔS	Applied nominal membrane stress range [MPa]
$\Delta\sigma_k$	Effective notch stress range [MPa]
σ_I	Primary residual stress [MPa]
σ_{II}	Secondary residual stress [MPa]
σ_{III}	Tertiary residual stress [MPa]
σ_b	Bending stress [MPa]
σ_m	Membrane stress [MPa]
σ_{mean}	Mean stress [MPa]
$\sigma_{mean,eff}$	Effective mean stress [MPa]
σ_{res}	Residual stress [MPa]
σ_{surf}	Surface stress [MPa]
θ	Diffraction angle [rad]
BCC	Body-centered cubic
BCT	Body-centered tetragonal
FCC	Face-centered cubic
FAT	Fatigue class of nominal stress method
FAT _{char}	Characteristic fatigue class
FAT _{eff}	Effective fatigue class
FEA	Finite element analysis
GMAW	Gas metal arc welding
HAZ	Heat affected zone
HFMI	High frequency mechanical impact
HSS	High-strength steel
IIW	International Institute of Welding

LEFM	Linear elastic fracture mechanics
S-N	Stress-life
SCF	Stress concentration factor
SWT	Smith-Watson-Topper
UHSS	Ultra-high strength steel

1 INTRODUCTION

Fusion welding is among the most important and widely-used joining processes in modern engineering industries like aerospace, automotive and construction. Alongside with the global growth of steel and aluminum usage, welding has been increasing worldwide during the last decades. Simultaneously, a global demand of light-weight structures has emerged, and thereupon the steel industry has progressively been shifting to high-strength steels (HSS). Consequently, the development of these steels has been rapid and has even led to the establishment of a new term, ultra-high strength steels (UHSS), representing steels whose yield strength can largely exceed 1 000 MPa. An obvious conclusion from these two trends – increasing welding and increasing material strengths – is that there is a real need for scientific knowledge and research of the strength properties of welded UHSS joints.

Strenx 1100 Plus is a UHSS which has good weldability in terms of modest softening at the heat-affected zone (HAZ), good static strength at the HAZ, and low hydrogen cracking susceptibility (SSAB 2020). However, under alternating load, the welds are susceptible to fatigue: most steel structure failures that lead to rupture are caused by fatigue phenomenon (Niemi 2003, p. 93). Welded structures are especially fatigue-prone, due to the material defects, tensile residual stresses and sharp geometrical notches caused by welding. The high yield strength of the material can lengthen the crack initiation life, but since micro defects caused by welding already often exist at fatigue-critical areas as weld toes, the total fatigue life of a welded joint may consist almost entirely of crack propagation. Hence, the fatigue lives of welded UHSS joints are often not substantially longer than those made of mild steels. This makes the fatigue study of welded UHSS structures one of the most important research topics of the field.

It is widely known that one essential parameter that affects the fatigue strength of a welded joint is the residual stress state at weld toe or root (Farajian et al. 2014, p. 178). In general, tensile residual stresses are detrimental to fatigue strength, whereas compressive residual stresses have a favourable effect (Radaj 1992, p. 320). In welded structures, tensile residual stress typically prevails against compressive, and the magnitude of these stresses can reach the yield point of the material (Sonsino 2009a, p. 88). As UHSS's have extremely high yield

strengths, the residual stresses in weldments in these steels also tend to be consistently high. This work investigates the formation and categorization of residual stresses in a welded UHSS joint. In particular, the effects of welding boundary conditions on the residual stress state and the final fatigue life are studied. By boundary conditions is here primarily meant the degree of restraint on welding deformations.

1.1 Research problem

Typically, the fatigue strength assessment of welded joints is done by performing tests with small scale laboratory specimens, in which restraint due to geometrical stiffness is most often very small or negligible. During welding and cooling, the specimen is allowed to deform freely, and thereby only local residual stresses due to uneven plastic strain distribution are developed in the vicinity of the weld (Masubuchi 1993, p. 1094). However, in many real-life welded structures, the structure itself has reasonably high geometrical stiffness. Most global scale welding distortions are obstructed by this stiffness, and global “reaction” stresses due to these restrained deformations remain in the structure after the cooling of the weld. These reaction stresses are almost inevitably present in accessory and repair welds. The reaction stresses are superimposed on the local residual stresses, and supposedly have a notable effect on the fatigue performance of the joint by increasing the effective stress ratio.

Design codes, like Eurocode 3 and recommendations of the International Institute of Welding (IIW), assume in general that welding residual stresses reach the yield strength of the material (EN 1993-1-9 2005, Hobbacher 2008). Residual stresses are also treated in equal fashion as mean stresses from external loading, which differ from residual stresses in source, distribution and relaxation behavior. (Farajian 2013, pp. 158–159.) Due to these simplifications, the residual stress state cannot be inserted as a parameter into the calculation formulas of these codes, but instead, general design stress-life (S-N) curves are used. These design curves have been compiled on the basis of fatigue tests performed with small scale specimens in pulsating tension with stress ratio $R = 0.5$ (Hobbacher 2008, p. 81, Sonsino 2009b, p. 65, Farajian 2013, p. 159.) Obviously, these curves cannot accurately reflect to differences in welding restraint conditions. Hereby, an erroneous view on the benefits of UHSS steels may arise, and additionally, risk for non-conservative fatigue design increases.

1.2 Aims

The primary aim of this work is to study how different welding boundary conditions affect the residual stress profile and the fatigue life of a welded UHSS joint. The secondary aim is to gain deeper understanding about the different roles of local residual stresses and global reaction stresses in fatigue crack initiation, propagation and final fracture. The tertiary aim is to make a novel proposal for the decomposition of the total residual stress distribution into components at the weld toe, categorized according to in what dimensions they self-equilibrate. This tertiary aim will serve future research purposes.

1.3 Research questions

This study seeks to answer the following research questions:

- 1) How do the welding boundary conditions affect the fatigue strength of a non-load carrying fillet joint?
- 2) How do the welding boundary conditions affect the residual stress state of a non-load carrying fillet joint?
- 3) Do global reaction stresses have a different role in fatigue phenomenon compared to local residual stresses?
- 4) Does the notch effect of the weld give local raise to global reaction stresses?

1.4 Methods

Answers to the research questions are sought by conducting experimental laboratory fatigue tests and numerical fatigue strength assessment. In the tests, a transversal attachment is fillet-welded on a UHSS plate having minimum yield strength of 1100 MPa. Three different restraint conditions are created for welding: unconstrained, fixed and semi-rigid (Figure 1). These different restraint conditions produce also different residual stress profiles to the joint area. The welded detail itself is identical in all restraint cases.

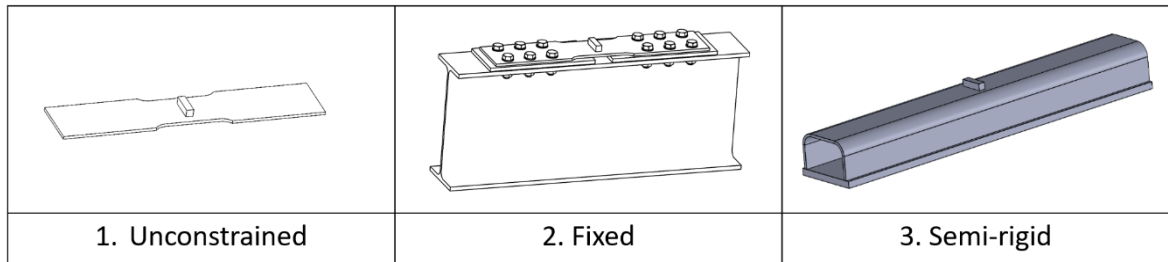


Figure 1. Welding boundary conditions.

The residual stress profiles at the weld toe areas are measured with X-ray diffractometry, and the fatigue lives are assessed by fatigue tests under constant load amplitude and uniaxial loading. Several different stress ranges and stress ratios are applied in the tests. In addition to the experimental tests and numerical assessment, a short literature review is made into recent research in the field.

1.5 Delimitations

All studied structures are made of Strenx 1100 Plus, and Union X96 is used as weld filler material. Since the intention is not to study the effects of welding parameters or weld geometry, all welds are welded with same parameters with gas metal arc welding (GMAW) process. All welds are non-load-carrying fillet welds, and only weld toe fatigue is of interest. All fatigue tests are made with constant amplitude uniaxial loading. Only normal residual stresses that are transverse to the weld are measured and taken into account in the study. Residual stress relaxation during the fatigue process will not be measured or investigated.

In fatigue phenomenon, the affecting factors are many, but this work focuses on the effects of residual stresses. Geometrical and metallurgical factors are mentioned but not more widely discussed. The nature of this work is experimental, and therefore neither welding nor the formation of the residual stresses are simulated. FEA is utilized only to determine the stress concentration factors for the fatigue life evaluation. A minor literature review is made, but it only has secondary role in this work.

2 FATIGUE OF WELDED JOINTS

Metal fatigue is a phenomenon which includes the nucleation and gradual propagation of a crack in the metal, and finally the fracture when the crack has grown to critical size. Fatigue phenomenon occurs under alternating load, when load peaks are below the ultimate strength of the material (Niemi & Kemppi 1993, p. 229.)

2.1 Fatigue phenomenon

The fatigue process consists of three main stages: crack nucleation, crack propagation and final fracture. Nucleation involves in short that under alternating load, local dislocation movements finally produce a small initial crack to an originally uncracked material. Crack propagation stage follows after nucleation: at this stage, the crack grows at a propagation rate which is related to the stress intensity range ΔK . (Dowling 2003, pp. 564-567.) The third stage is final fracture: the remaining cross section fails either by brittle fracture or ductile failure. This occurs when the propagating crack has diminished the load-carrying cross section so that the remainder no longer withstands the greatest load peak (Niemi & Kemppi 1993, p. 238).

2.2 Crack nucleation

In fatigue crack nucleation, a small initial crack is formed at the surface of the material, when the material experiences repeated, alternating local plastic deformation. When observed at macroscopic scale only, the alternating strains seem to eliminate each other at every load cycle. However, when observed at microscopic scale, it can be noted that the alternating strains produce slip bands in those grains which are unfavourably oriented with respect to the loading direction. Some of these slip bands develop into single-grain cracks which may, as the alternating load continues, cross the grain boundaries, coalesce and finally develop into macroscopic flaws in the material. Such a macroscopic flaw is called a nucleated (initiated) fatigue crack. Typically, a fatigue crack nucleates at a location of already existing material defect such as inclusion, impurity, slip band, welding defect or surface scratch. (Dowling 2013, p. 436.)

The duration of the nucleation stage depends – among other factors – on the local stress range: the higher the stress range, the shorter the crack initiation life (Dowling 2013, pp. 435–439). On the other hand, mean stress has not proved to have a very significant effect. Also the quantity, magnitude and quality of the initial material defects tend to have an effect on the initiation life, together with several other material characteristics. Some controversy exists on when the nucleation stage can be considered ended and propagation stage begun. One proposed definition is that the crack has nucleated, when the crack size allows the application of linear elastic fracture mechanics (LEFM) to the assessment of crack growth. (Niemi & Kemppi 1993, p. 256.)

2.3 Crack propagation

Once nucleated, the crack grows (propagates) in a plane perpendicular to the major principal stress (Berge 1985, p. 161). The most important mathematical tool that is commonly applied to crack propagation modelling is LEFM. One of the cornerstones in LEFM application to crack growth simulation is the *Paris law*, which states that at certain stress intensity levels, the crack propagation rate da/dN is directly related to a power of the stress intensity range, and thus it can be calculated from formula (Dowling 2003, pp. 564-567):

$$\frac{da}{dN} = C \cdot (\Delta K)^m \quad (1)$$

where C and m are material constants, and ΔK is the stress intensity range. The stress intensity factor K is a function of crack size and shape, the remotely applied stress, and the crack opening mode (Figure 2). The opening mode is determined from the crack tip position with respect to the load. (Dowling 2013, pp. 339–344.)

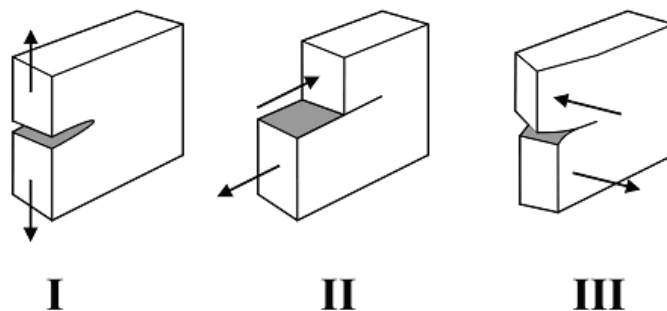


Figure 2. Crack opening modes (Sanford 2003, p. 57)

Formulas can be derived for the determination of distinct stress intensity factors for each opening mode, and more than one opening mode can be present simultaneously in the same crack (Dowling 2013, p. 344.). However, mode I is typically dominating. In case opening modes II or III are present, the crack tends to change its path and position so that mode I again dominates. For this reason, it is often sufficient that the stress intensity factor for opening mode I is determined. (Sanford 2003, p. 57.)

2.4 The impact of welding on fatigue strength

In general, it can be with confidence stated that for almost any structural detail, welding reduces the fatigue strength. This is due to at least four phenomena which occur: Firstly, welding produces material defects to the structure. In the as-welded condition, flaws of magnitude of 0.2–0.3 mm may be found in the weld toe and root areas. Fatigue cracks tend to nucleate or directly grow at the bottoms of such flaws much more rapidly than in the smooth material. (Niemi, Kilkki, Poutiainen & Lihavainen 2004, p. 11.) In such cases, the crack nucleation stage remains relatively short, and the total fatigue life may consist almost entirely of the crack propagation stage (Niemi & Kemppi 1993, p. 229). Thus, the total fatigue life of the weld becomes shorter than that of the plain base material.

Secondly, welding usually produces high tensile residual stresses, which have a deteriorating effect on the fatigue strength (Radaj 1992, p. 320; Kirkhope et al. 1999, p. 456; Farajian et al. 2014, p. 178). Irrespective of the welding boundary conditions, some residual stress components are always formed as a consequence of welding, due to the unevenly distributed plastic and thermal strains.

Thirdly, in most cases the weld itself forms a geometrical discontinuity and a sharp notch in the structure, which causes local stress concentration known as the notch effect. Fourthly, due to welding heat input and unfavourable cooling rate, softening occurs at some areas in the HAZ with certain steel grades, such as direct quenched UHSS's. The softening implies a decrease in the material's tensile strength, which leads to a reduced initiation life capacity at the weld toe and root, which are the most probable crack initiation sites.

2.5 The impact of mean stress on fatigue strength

It has been generally recognized that increasing mean stress (i.e., increasing the stress ratio) decreases the fatigue life of the structure, whereas a reduction in mean stress increases the fatigue life. Yet, in welded structures, the mean stress effect is not so pronounced, due to the high tensile residual stresses which often are present in weldments. When considering the mean stress effect, the affecting variable is *effective* mean stress. Traditionally it has been understood that the effective mean stress has little effect on fatigue crack nucleation, but it has a significant effect on the fatigue crack growth rate (McClung 2007, p.174). The effective mean stress $\sigma_{mean,eff}$ consists of applied mean stress σ_{mean} and residual stress σ_{res} (Hensel, Nitschke-Pagel & Dilger 2017, pp. 999–1000):

$$\sigma_{mean,eff} = \sigma_{mean} + \sigma_{res} \quad (2)$$

The residual stress σ_{res} may originate either from the heat effects of welding, or from structural restraints. It is to be noted that σ_{mean} is very often force-controlled, since it originates from externally applied load. Contrarily, σ_{res} is regarded as displacement-controlled, and it partly relaxes due to crack propagation (McClung 2017, p. 193). In addition, relaxation due to either monotonic or cyclic yielding occurs in given circumstances. However, in fracture mechanics, residual stresses are usually treated similarly as externally applied mean stresses, which introduces some error in the fatigue life assessment, unless the relaxation behavior is taken into account (Hensel et al. 2018, pp. 125, 130).

2.6 Fatigue evaluation methods

Today, several fatigue assessment methods exist to predict the fatigue life of a welded joint. Among them are the nominal stress, structural stress, effective notch stress, local strain and LEFM methods. In addition to these, the newly proposed 4R method represents the state of the art in the field, and it has proven to be an effective means of fatigue life evaluation. In this study, the nominal stress method and the 4R method are introduced and used.

2.6.1 Nominal stress method

In the nominal stress method, the general stress range in the structure at a further distance from the weld is determined. Design codes as EN 1993-1-9 and IIW recommendations present S-N curves (fatigue classes) for different welded detail categories (EN 1993-1-9 2005, pp. 20–29; Hobbacher 2008, pp. 46–74). The fatigue life is assessed by selecting the

detail category which represents the actual detail, and the fatigue life is then evaluated using the S-N curve of that particular detail category and the nominal stress range in the structure. In the nominal stress method, no geometrical discontinuities, welding imperfections, small geometrical details or mean stresses can be entered into the calculation as parameters. The effects of these variables have been embedded in the S-N curves, based on several worst-case assumptions. (Niemi & Kemppi 1993, p. 246.)

For welded joints, the nominal stress method of EN 1993-1-9 does not allow the separate consideration of applied mean stresses. On the other hand, IIW recommendations allow *fatigue class enhancement* for small-scale and thin-walled structures containing short welds, or for stress-annealed welded components; the fatigue class of the detail category may be multiplied by an enhancement factor that varies between 1.0–1.6. The enhancement factor depends on the *effective stress ratio*, that is, the combined effect of residual stress and applied mean stress. (Hobbacher 2008, p. 81.)

2.6.2 4R method

The 4R method was originally developed by D.Sc. (Tech) Timo Nykänen and his research group in LUT University. The method was derived by curve fitting into a large basis of test results obtained from literature (Nykänen & Björk 2015; Nykänen & Björk 2016). Since the days of Nykänen, the method has been further developed and elaborated by the researchers of the LUT Laboratory of Steel Structures. The 4R method is an accurate technique for fatigue life evaluation, and it takes into account the most important and easily measurable factors that affect the fatigue strength of a welded joint. The 4R method receives as calculation parameters the effective notch stress range $\Delta\sigma_k$, and the four R's (Björk et al. 2018, p. 1286):

- R_m (ultimate strength of material)
- Radius (actual toe or root radius)
- Residual stress (residual stress at toe or root)
- R (stress ratio from external load)

First, the local stress-strain response at the weld toe or root is computed by means of local strain approach, Ramberg-Osgood material model and Neuber's notch theory, to determine the local stress ratio R_{local} at the critical notch. The 4R method applies the Smith-Watson-

Topper (SWT) mean stress correction equation and R_{local} to calculate the final fatigue life N_f (Björk et al. 2018):

$$N_f = \frac{C_{ref}}{\left(\frac{\Delta\sigma_k}{\sqrt{1 - R_{local}}} \right)^{m_{ref}}} \quad (3)$$

where C_{ref} is the fatigue capacity and m_{ref} is the slope of the reference curve. The effects of the residual stresses, as well as the externally applied mean stress, are accounted for in the calculation of R_{local} . Thus, the 4R method serves as a reasonable fatigue life evaluation tool when the effects of residual stresses on the fatigue strength of welded joints are studied.

3 WELDING RESIDUAL STRESS

The theory of welding residual stresses is discussed in this chapter; the nature and formation of residual stresses due to fusion welding are introduced. In addition, the effects of residual stresses on the fatigue life of welded joints are discussed. Also a very short review is made to recent research on residual stress effects on the fatigue of weldments.

3.1 Residual stress

By definition, residual stresses are self-equilibrating stresses that exist in a body or structure without the presence of externally applied loads. Residual stresses are always self-equilibrating; when the body is not subjected to external load, both the resultant force and resultant moment of the stresses in the body are equal to zero. When external load is applied, the stresses caused by the load are superimposed on the residual stresses existing in the body. (Masubuchi 1980, pp. 92–94; Radaj 1992, p. 5.)

Traditionally, residual stresses have been categorized into first, second and third order stresses. The second and third order stresses (microscopic stresses) act over microscopic areas, as between single grains, grain subregions or even atomic areas. The first order stresses (macroscopic stresses) act over macroscopic areas of multiple grains. (Masubuchi 1980, p. 92; Radaj 1992, pp. 5–6.) The microscopic stresses are mostly studied in the field of materials science, whereas in engineering practice and in this study, only macroscopic residual stresses are of interest.

In general, there are two mechanisms to produce residual stresses to a body or structure (Masubuchi 1993, p. 1095):

- 1) Uneven distribution of plastic strains
- 2) Structural mismatch.

Based on the generation mechanism, the macroscopic residual stresses can be further categorized: both Masubuchi (1980) and Radaj (1992) present the categorization into “constraint stresses” which are in local self-equilibrium, and “reaction stresses” which are in equilibrium with the support reactions provided by stiff structure or assembly.

Welding residual stresses can be either tensile, arising from the restrained thermal contraction of the heated zone, or compressive, caused by the solid-state phase transformation of the cooling weld metal. Both need to be considered to determine the exact residual stress state at potential fatigue crack initiation sites such as weld toes and roots.

3.2 Tensile welding residual stresses due to thermal contraction

Fusion welding introduces steep temperature gradients to the base material surrounding the fusion zone. This leads to strongly inhomogeneous strain field in the vicinity of the weld: the heat expansion of the intensely heated material causes compressive strains. This heat expansion is restrained by the surrounding colder material. Due to the elevated temperature, compressive yielding occurs at relatively low stress levels in the heated material, that is, the heated regions deform plastically due to the hindered thermal expansion. (Hensel et al. 2018, pp. 125–126; Radaj 1992, p. 8.)

While cooling, thermal contraction occurs in the heated material, and this contraction is again restrained by the surrounding material which has experienced milder temperature change. During cooling, the yield strength and Young's modulus of the material increase, and, as a result, tensile residual stress develops in the material due to the restrained contraction. Equilibrating compressive component is developed in the surroundings. Residual stresses are formed in three dimensions: in longitudinal, transverse and through thickness direction. Figure 3 shows the schematic distributions of longitudinal and transverse shrinkage stresses in a butt joint. The transverse residual stresses are of most interest, because loading typically occurs in the direction transverse to the weld. In such a case, the crack propagates along the weld toe or root, and the transverse residual stresses serve as crack opening stresses. (Hensel et al. 2018, pp. 125–126; Radaj 1992, pp. 8–11.)

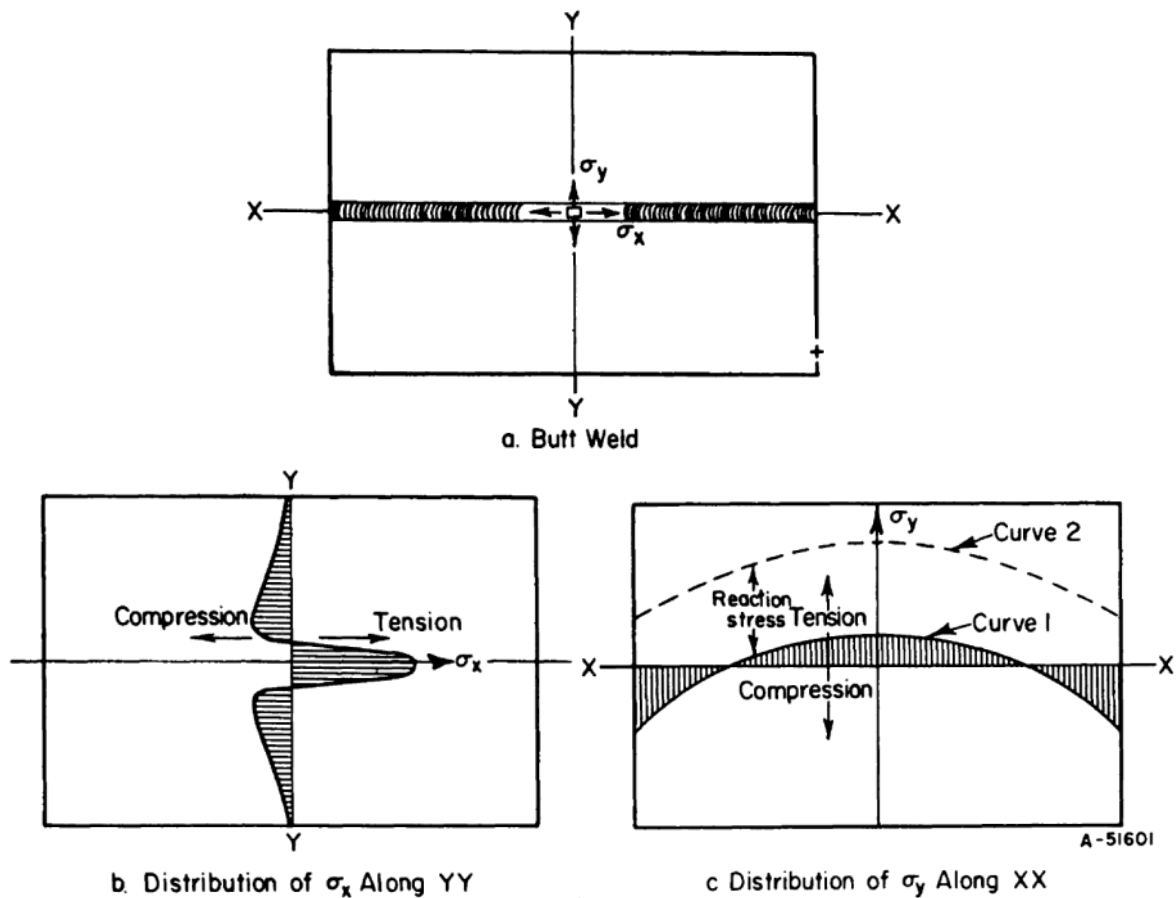


Figure 3. Schematic representation of (b) longitudinal and (c) transverse welding residual stresses in a butt joint (Masubuchi 1980, p. 192).

3.3 Welding residual stresses due to phase transformation

While cooling down from austenitization temperature, most steels experience solid-state phase transformation from austenitic face-centered cubic (FCC) lattice to body-centered cubic (BCC) crystalline structures like ferrite, or even body-centered tetragonal (BCT) structures like martensite. Body-centered structures are less optimally packed lattices and thus require more volume compared to face-centered structures. Hereby, the transformation from face-centered into body-centered structure causes volumetric expansion in the material. (Callister & Rethwisch 2011, pp. 356–365.) This expansion is restrained by the surrounding material which has undergone a different temperature history. If this restrained expansion occurs at low enough temperature so that high enough yield strength and Young's modulus have developed in the material, a compressive residual stress component is formed. This phase transformation-induced compressive stress component is superimposed on the tensile stress component from the hindered shrinkage. The phase transformation-induced compressive stresses are often present at fatigue-critical areas as weld toes, and they have

positive effect on the fatigue strength of the weld. (Hensel et al. 2018, p.126, Radaj 1992, pp. 8–10.) With most weldable steels, the final residual stress state is a combination of thermally-induced tensile and phase transformation-induced compressive stress. The final total residual stress can be either tensile, zero or compressive, depending on the solid-state phase transformation temperature, material yield strength, etc. (Farajian et al. 2014, p. 179).

3.4 Impact of residual stress on fatigue strength

The effects of residual stresses on the fatigue strength of welded joints have been researched in numerous studies. The research shows that in general, tensile residual stresses have been proven to decrease fatigue strength, whereas compressive residual stresses have favourable effect on fatigue strength (Radaj 1992, p. 320). In essence, the residual stresses affect the local effective stress ratio: local mean stress is increased by tensile and decreased by compressive residual stress (McClung 2007, p. 174).

According to Farajian et al. (2013), the deteriorating effects of tensile welding residual stresses on fatigue strength have been recognized and reported as early as in late 1950s (Kudryavtsev 1956). The favourable effect of compressive residual stresses has also been verified by several researches, and it has also been acknowledged and included in some design codes. For example, IIW recommendations state that by introducing compressive residual stress by means of hammer or needle peening, an enhancement of the fatigue class by factor of 1,5 is allowed at the highest (Hobbacher 2008, p. 88).

3.5 Measurement of welding residual stress

In measurement of welding residual stress, at least following types of techniques are used (Masubuchi 1980, p. 112):

- 1) Stress-relaxation techniques
- 2) X-ray diffraction techniques
- 3) Neutron diffraction techniques
- 4) Techniques exploiting stress-sensitive properties.

In this study, residual stresses are measured using X-ray diffraction technique only.

The stress relaxation techniques are all destructive methods. They rely on measurement of elastic strain release due to stress relaxation, which occurs as a consequence of material

removal. The material is typically removed by machining (milling, drill boring, etc.). The relaxation strains are commonly measured with electric strain gauges which have been glued to the material surface prior to the material removal. Strain data is collected from several successive material removals, whence the stress relaxation history can be determined. Finally, the residual stress state of the original, unmachined specimen can be deduced from the strain history results. (Masubuchi 1980, pp. 112.)

The techniques using stress-sensitive properties are non-destructive. These methods are based on measurements of properties that are known to be related to the material stress state, such as material hardness or polarization of ultrasonic wave, from which the stress state can be indirectly deduced. (Masubuchi 1980, pp. 112–113.)

3.5.1 X-ray diffraction measurement of welding residual stress

The X-ray diffraction technique is a non-destructive method of residual stress measurement. It utilizes the metallic lattice structure of the material and the diffraction phenomenon of a reflected electromagnetic beam: In metals that have crystalline microstructures, elastic strains cause changes in the crystalline lattice. These changes in the lattice cause change of the lattice parameter (=unit cell edge length). Hereby, the strain state of the material can be determined by measuring the lattice parameter in the strained state using X-ray diffractometry, and then comparing this measured parameter with the lattice parameter of the unstressed material, which normally is a material constant. (Masubuchi 1980, p. 112; Callister & Rethwisch 2011, p. 76.)

The X-ray diffraction method has its basis in *Bragg's law of diffraction* which can be stated as follows (Callister & Rethwisch 2011, p. 76):

$$n\lambda = \frac{a}{\sqrt{h^2 + k^2 + l^2}} \cdot 2 \sin \theta \quad (4)$$

Where λ is the X-ray wavelength, n is the order of reflection $\{1, 2, 3, \dots\}$, θ is the diffraction angle, h , k and l are the Miller indices, and a is the lattice parameter of the cubic unit shell. Equation 4 states the relationship between the lattice parameter, diffraction angle and beam wavelength. Thus, the lattice parameter can be computed based on the X-ray diffractometry

results: once the wavelength is known, the lattice parameter a can be determined from the beam diffraction pattern.

One major disadvantage of X-ray diffractometry is that it is time-consuming. The method has also proven to be somewhat inaccurate, particularly if the atomic structure of the material has been distorted by large temperatures, as the case is with welded specimens. (Masubuchi 1980, p. 113.) An additional shortcoming of the technique is that the strain state can be measured at the material surface only, and thus the through thickness distribution cannot be determined using X-ray diffractometry alone. The through thickness distribution is generally needed for crack propagation analyses (Hensel et al. 2018, p. 126).

3.5.2 Neutron diffraction measurement of welding residual stress

The neutron diffraction technique is also a non-destructive method, and it is based on same physical principles as the X-ray diffraction technique: The diffraction pattern of a reflected beam of neutrons is studied to determine the distances between atomic layers in the crystalline lattice. Same Bragg's law is utilized as in X-ray diffraction (see chapter 3.5.1).

Neutron diffraction differs from X-ray diffraction in that a neutron beam is used instead of an X-ray beam. The neutrons for this purpose are created by spallation or fission (Paranjpe 2005, p. 2). Since neutrons are smaller than the wavelength of X-rays, the neutron beam has deep penetration, and the neutron diffraction method allows investigation of atomic layers deeper in the material. This creates the main advantage of neutron diffraction method over the X-ray diffraction method: With neutron diffraction, the residual stress distribution can be measured also in the depth of the material in thick specimens, whereas the X-ray diffraction method is capable of surface measurements only. Yet, neutron diffractometers are expensive and are currently found only in several dozens of laboratories and facilities in the world. (Paranjpe 2005, pp. 1–2.)

3.6 Recent research into residual stress effects on fatigue

This chapter shortly summarizes some of the former research on fields which are closely related to the topic of this thesis; the effect of residual stresses on the fatigue strength of welded joints, the impacts of different welding boundary conditions, and residual stress categorization.

Hensel et al. (2016) have studied non-load-carrying longitudinal gusset welds. According to the results, the fatigue strength of the joint was almost doubled by relieving the residual stresses by means of annealing. In the named study, welding distortions were removed before the fatigue test, in order to avoid second-order bending stresses. Externally applied stress ratios $R = -1$ and $R = -3$ were used. In earlier studies, annealing had not improved fatigue strength because annealing increased welding distortions, which led to higher clamping bending stresses which are detrimental to the fatigue life of the specimen. Overall, the local transverse residual stress was noted to be highest at the weld centerline and noticeably lower at the weld toe.

Farajian et al. (2014) have researched welded small-scale specimens with low transverse stiffness and compared the results with large-scale specimens which have high transverse stiffness (Figure 4).

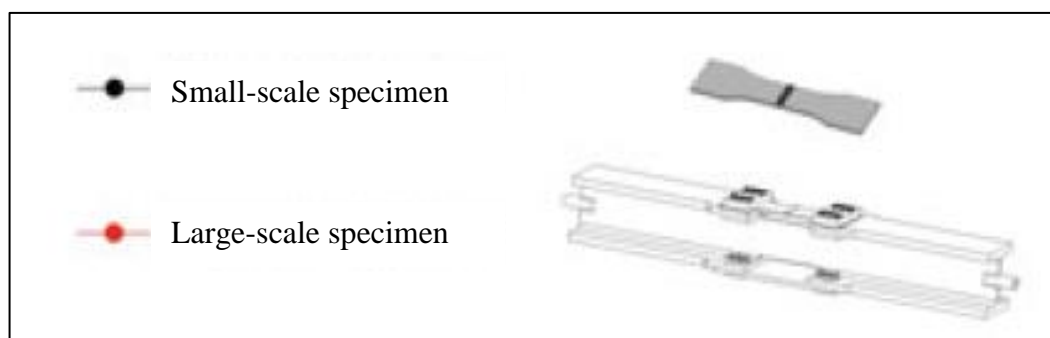


Figure 4. Small-scale and large-scale specimens (Farajian et al. 2014, p. 193).

A definite difference between the residual stress profiles of small-scale and large-scale specimens was recognized. In the small-scale specimens, residual stresses up to 60 % of material yield strength were observed, the ratio growing alongside with the yield strength. In large-scale specimens, residual stresses up to 80 % of yield strength were recorded. With

HSS's such as S690 and S960, the ratio between residual stress and material proof strength ($\sigma_{res}/R_{p0.2}$) was lower than with mild steels. With S355, a parallel shift of ca. +300 MPa in the residual stress profile was observed when going from small scale specimens to the stiffer large-scale specimens (Figure 5).

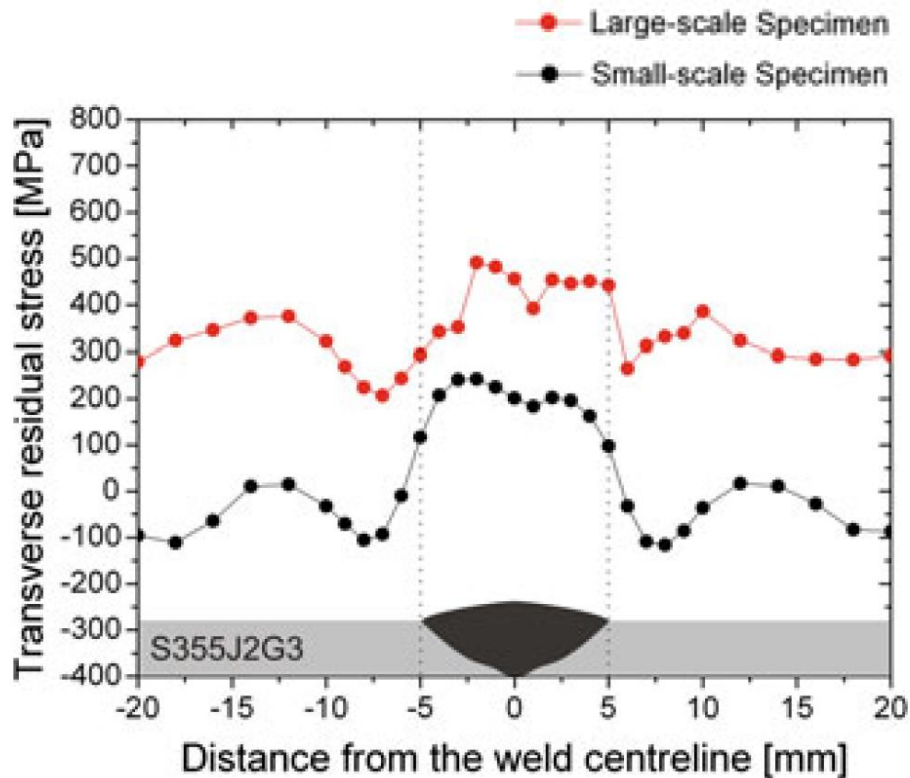


Figure 5. Residual stress profiles of joints with different stiffness (Farajian 2014, p. 193).

The relaxation of tensile residual stresses was more pronounced with large-scale specimens (Farajian 2014, pp. 195–198). Unfortunately, the fatigue life test results of this study have not been accessible to the author of this thesis.

Hensel et al. (2018) made literature survey on the impact of welding residual stresses on the fatigue performance of structures. In this paper, welding residual stresses were categorized to type A (local, short-range, residual stress) and type B (global, long-range, reaction stress). Type A stresses develop due to internal strain mismatch during cooling, whereas type B stresses occur due to restraint in the overall structure. The exact categorization criterion is: Type A stresses are in equilibrium across the section potentially containing the crack, and in type B stresses, the equilibrium exists only over the complete structure. Such categorization is made because in fracture mechanics, short-range and long-range residual stresses are

treated in different ways. However, the (assumedly) different roles of these two types in fatigue crack nucleation and propagation have not been concluded, that is, no experimental or simulation results have been reported in this study that would utilize this categorization and prove such categorization to be necessary. (Hensel et al. 2018, pp. 123–126.)

Based on existing research results, the authors state – in agreement with Hensel et al. (2016) – that high tensile residual stresses are typically found in the weld metal itself, but at weld toe regions, much lower tensile or even compressive residual stresses have been observed. This is contradictory to older literature, where high tensile stresses at weld toes are assumed as a default. This has been due to the ignorance of the effects of solid-state phase transformation, and also to the lack of residual stress measurements in the past. (Hensel et al. 2018, p. 126.)

Two major problems are noted in the residual stress categorization proposed by Hensel et al (2018): Firstly, challenges are met when the measured residual stress distribution is to be decomposed into components consisting purely of type A or type B stresses. Secondly, some interdependencies may arise between types A and B, especially with “self-restraint” specimens like longitudinally stiffened plates. These interdependencies cause difficulties in the categorization. (Hensel et al. 2018, pp. 134–135.)

Hensel, Nitschke-Pagel & Dilger (2015) made experiments with longitudinally stiffened plates and deposit welds on non-stiffened plates. The number of weld passes was varied. Residual stresses were measured both with X-ray and neutron diffractometry. The results showed that relatively low tensile residual stresses developed at weld toes. Instead, higher residual stress peaks were observed at 1–5 mm distances from the toe. It was also noticed that the residual stresses are dependent on both geometrical stiffness and welding heat input: tensile residual stresses increase with slow cooling time and high outer restraint, both of which conditions are unlikely when welding small laboratory-scale specimens. The effect of the cooling time is explained by higher influence of the phase transformation-induced hindered expansion when fast cooling occurs. The achieved fatigue lives in testing were not reported, but it is stated that they are in good accordance with existing literature. (Hensel et al. 2015.)

Schroepfer & Kannengiesser (2014) made experimental testing by multi-pass butt-welding with both restrained and unrestrained specimens. Inter-pass temperatures and welding parameters were varied, which resulted in different cooling times. The results are in agreement with Hensel et al. (2015): Slow cooling rate, caused by high heat input and high inter-pass temperatures, produces high tensile residual stresses. The same phenomenon was observed both in the free and restrained specimens. The transverse residual stresses at the weld toe region were clearly higher in the free specimens than in the restrained specimens when measured in the de-clamped state (Figure 6).

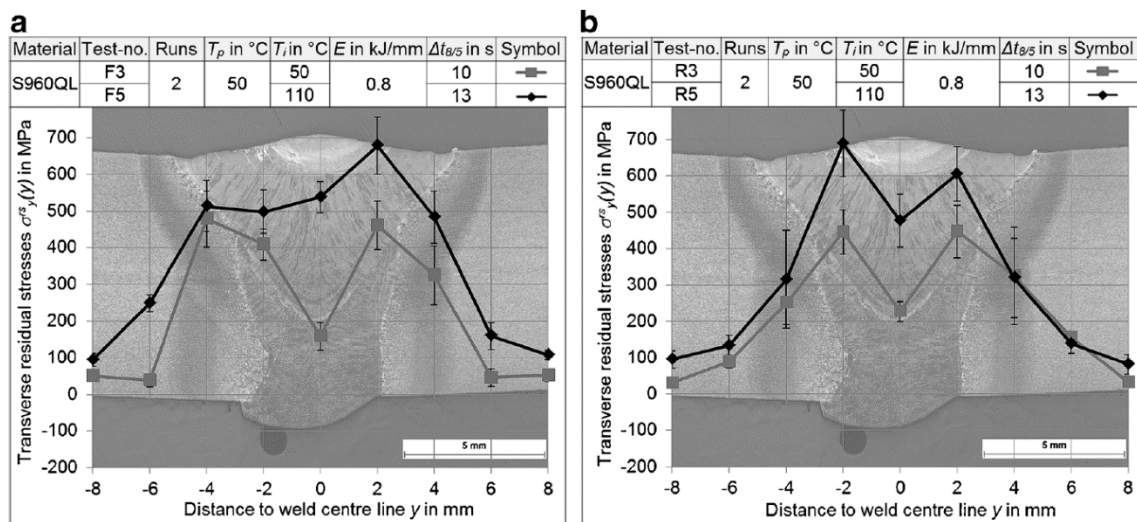


Figure 6. Transverse residual stresses for two interpass temperatures in (a) free specimen and (b) restrained specimen in de-clamped state (Schroepfer & Kannengiesser 2014, p. 429).

The nominal reaction stresses in the restrained specimens were calculated from the measured restraint forces and the cross section dimensions. After this, the residual stress state in the clamped condition was estimated by superpositioning this reaction stress onto the measured residual stress profile of the de-clamped state. The obtained total stresses for the restrained specimens were higher than those of the free specimens.

4 RESIDUAL STRESS CATEGORIZATION

The classification into microscopic and macroscopic residual stresses has already been introduced in this work in chapter 3.1. In this chapter, only macroscopic residual stresses and their further categorization are discussed. Firstly, the existing categorization criteria are presented as found in the literature. Secondly, a novel proposal is made for the categorization: three categories can be distinguished according to the different self-equilibrium conditions.

4.1 Existing categorization of macroscopic residual stresses

Hensel et al. (2018) have summarized the present state of the art of residual stress categorization, which is shortly introduced here. As stated already in chapter 3.1, there are two primary mechanisms of residual stress creation: inhomogeneity of plastic strain field, and structural mismatch. Thereby, according to Masubuchi (1993, p. 1101), also welding residual stresses can be categorized by their creation mechanism as

- 1) Local welding residual stresses (Type A)
- 2) Global reaction stresses (Type B)

Type A residual stresses develop due to the inhomogeneous thermal and plastic strains caused by the welding heat input. These stresses exist in the vicinity of the weld, and they occur also in an unrestrained small-scale welded specimen. These stresses self-equilibrate over the cross section of the body. From fatigue point of view, hereby is primarily meant the cross section that potentially contains the crack. The fracture mechanics definition for these stresses is that they do not contribute to plastic collapse. (Hensel et al. 2018, pp. 125, 134.)

Type B residual stresses exist over the global structure and are caused by external restraint which obstructs the welding deformations. These stresses equilibrate with the support reactions of the external restraints (Table 1). When comparing small and large scale specimens, Farajian (2013) observed a parallel shift of the residual stress profile into positive direction (Figure 5), indicating that the type B residual stress could be superimposed on the type A stress profile without re-considering the notch effect of the weld. (Hensel et al. 2018, p. 125; Farajian 2013, pp. 11–12.) From fracture mechanics point of view, these stresses do

contribute to plastic collapse (Hensel et al. 2018, p. 134). The key differences between type A and type B residual stresses are listed in Table 1.

Table 1. Properties of residual stress categories (Hensel et al. 2018).

Type A residual stresses	Type B residual stresses
Are created by the inhomogeneity of plastic strains due to welding	Are created by external restraint which obstructs welding deformations
Act locally near the weld	Act globally over the structure
Self-equilibrate across the cross section	Equilibrate with the restraint support reactions
Do not contribute to plastic collapse	Contribute to plastic collapse
Are found in all welded specimens	Are found in welded structures with restraint

In general, design codes do not take into account the residual stress type. Yet, BS 7910 gives instructions for the calculation of stress intensity factors separately for self-equilibrating residual stress component (Type A) and bending and membrane residual stress components (Type B). (BS 7910 2013, pp. 383–384.)

4.2 New proposal for the categorization of macroscopic residual stresses

In this chapter, a novel proposal is made for the categorization of residual stresses. The leading idea is that the residual stress distribution in any structural detail can be decomposed into three components: primary (σ_I), secondary (σ_{II}) and tertiary (σ_{III}) stresses, according to the degree of locality of the self-equilibrium condition. A schematic representation of the through thickness distributions of these components is shown in Figure 7.

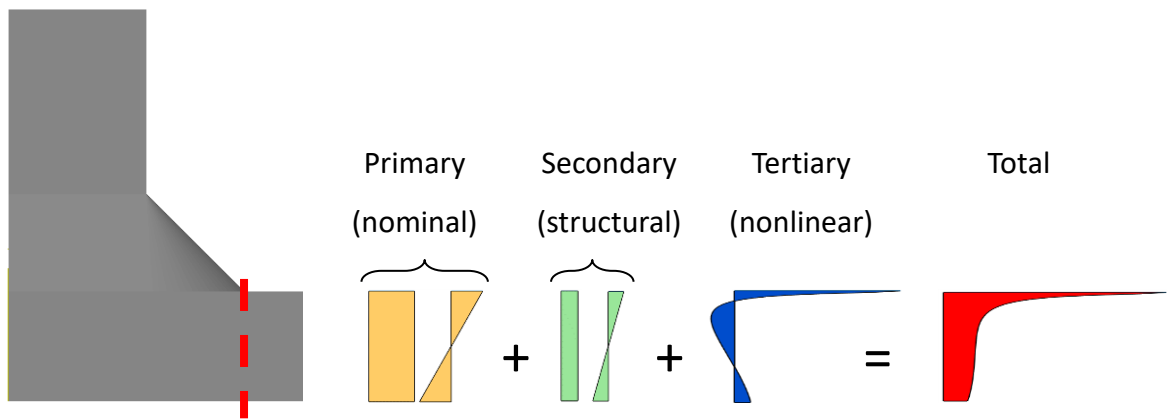


Figure 7. Schematic representation of the three residual stress components at a weld toe.

The primary and secondary components consist of membrane and bending parts, and the tertiary stress has a nonlinear, self-equilibrating distribution through thickness.

4.2.1 Primary residual stresses

Primary residual stresses are membrane and bending stresses that are in equilibrium with the global support reactions only (Figure 9). Figure 8 shows a schematic surface distribution of this case.

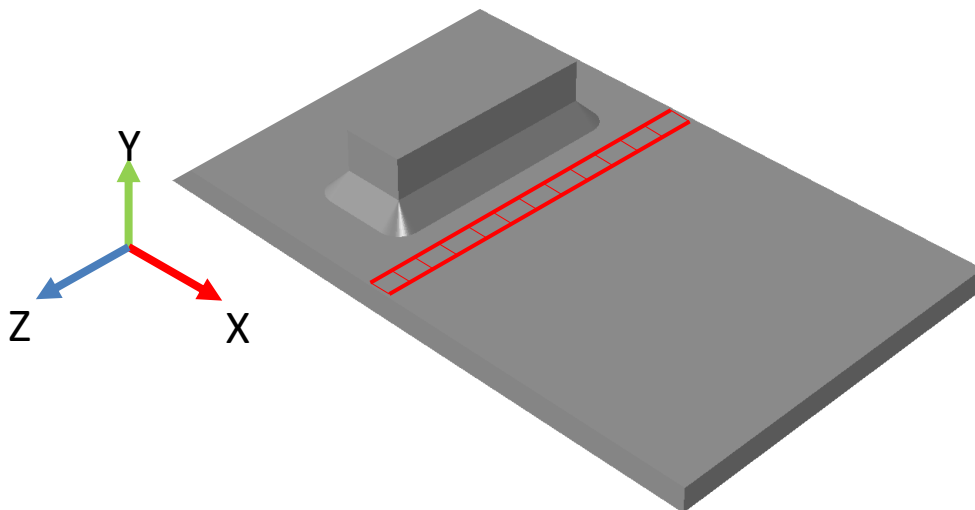


Figure 8. Schematic σ_l distribution at the surface.

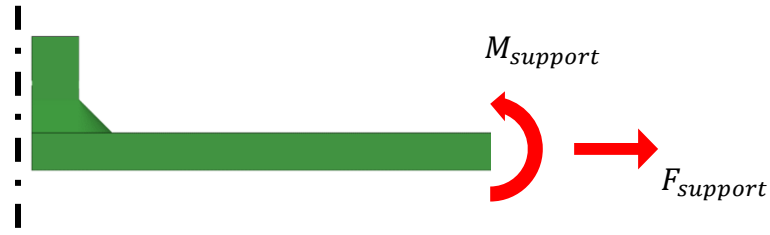


Figure 9. Global support reactions.

Primary residual stresses exist at any cross section of the specimen, and satisfy the condition that the resultant force and resultant moment over the cross section are equal to the global support reactions:

$$\frac{1}{bt} \int_D \sigma_I(y, z) dA = F_{support} \quad (5)$$

$$\frac{6}{bt^2} \int_D \sigma_I(y, z) \left(\frac{t}{2} - y \right) dA = M_{support} \quad (6)$$

where $F_{support}$ is support reaction force, and $M_{support}$ is support reaction moment (Figure 9). Following the categorization criteria of Hensel et al. (2018), the primary residual stresses fall into category “Type B” stresses. This stress component is present in a welded specimen which is a part of a larger and stiffer structure, where the stiffness of the structure provides the necessary support reactions. This is especially the case with repair welds and accessory welds in larger structures.

4.2.2 Secondary residual stresses

Secondary residual stresses are membrane and bending stresses which are locally in self-equilibrium across the specimen cross section (Figure 10). In fatigue analysis, the cross section which contains the crack is typically of interest; in the case of an all-around-welded accessory weld, this cross section is found at the weld toe.

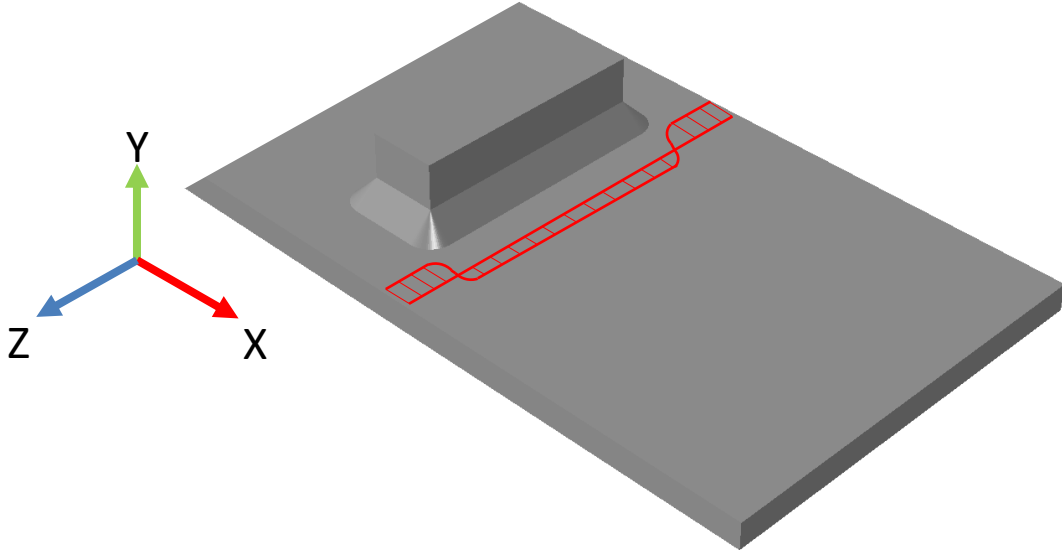


Figure 10. Schematic σ_{II} distribution at the surface.

The cross-sectional equilibrium is satisfied when both resultant force and resultant moment of the stresses in the particular cross section are equal to zero:

$$\frac{1}{bt} \int_D \sigma_{II}(y, z) dA = 0 \quad (7)$$

$$\frac{6}{bt^2} \int_D \sigma_{II}(y, z) \left(\frac{t}{2} - y \right) dA = 0 \quad (8)$$

where b is plate width, and D denotes the area of the discussed cross section. Following the categorization criteria of Hensel et al. (2018), also secondary stresses fall into category “Type A” stresses. Secondary stresses develop in a welded specimen whose cross section perpendicular to the welding direction is not constant. For example, Figure 10 represents an example of such specimen: the edges of the plate that are aligned in X-direction are preventing both axial contraction and angular distortion. Secondary residual stresses originate from this self-restraint.

4.2.3 Tertiary residual stresses

The tertiary residual stresses are locally in self-equilibrium in the through thickness direction. That is, at the critical cross section, the stress distribution along any line aligned with the Y-axis (Figure 11) is self-equilibrating. These stresses are created by the inhomogeneous thermal strain field into any welded specimen.

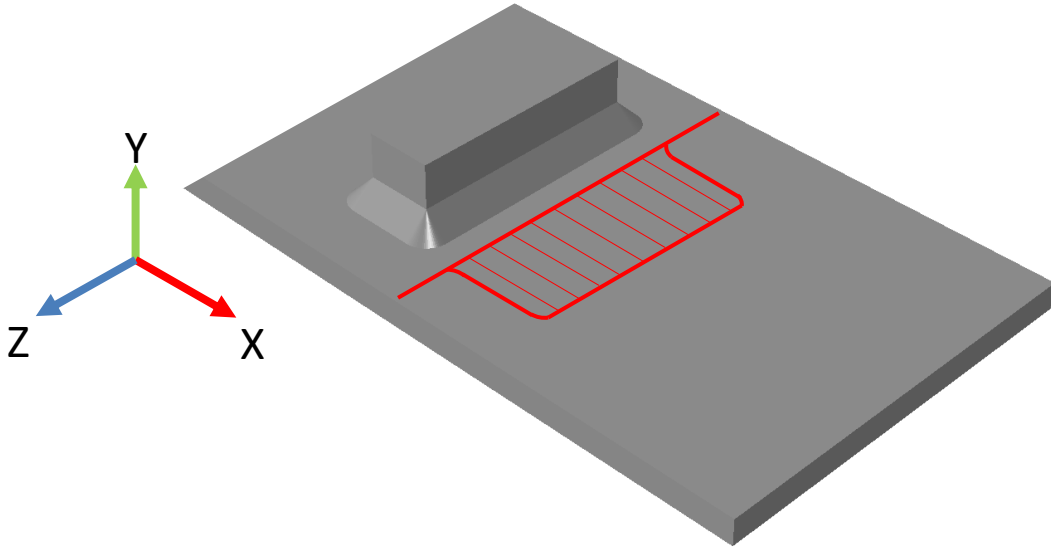


Figure 11. Schematic σ_{III} distribution at the surface.

In essence, tertiary stresses satisfy the following condition: At any cross section (typically the cross section that contains the weld toe), at each location Z_i , both resultant force and resultant moment of the through thickness distribution are equal to zero:

$$\frac{1}{t} \int_0^t \sigma_{III}(y, z) dy = 0 \quad \text{at any } Z \quad (9)$$

$$\frac{6}{t^2} \int_0^t \sigma_{III}(y, z) \left(\frac{t}{2} - y \right) dy = 0 \quad \text{at any } Z \quad (10)$$

where t denotes the plate thickness. Following the more traditional categorization criteria from Hensel et al. (2018), the tertiary stresses fall into category “Type A” stresses. If a relatively short butt weld is welded in a specimen whose cross section perpendicular to the

welding direction is constant (Figure 12), and the welding deformations are not prevented by any means, then ideally only the tertiary stress component will develop.

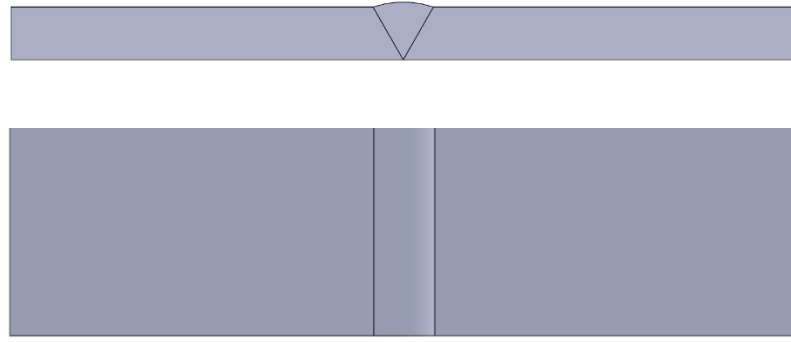


Figure 12. Example of welded specimen in which only tertiary residual stresses exist. All welding deformations occur freely without restraint.

5 MATERIALS AND METHODS

The main focus of this thesis is on experimental laboratory testing of weldments. Alongside with the tests, numerical fatigue analysis has also been made to complement the findings of the experimental tests.

5.1 Experimental testing

Experimental tests were made to study the effects of welding boundary conditions on the residual stress profile and fatigue strength of an accessory weld. Welding was performed under varying conditions of restraint. The surface residual stress profiles were measured with X-ray diffractometer, and the fatigue strengths were determined by constant amplitude fatigue tests under uniaxial loading.

The structural detail under investigation was a fillet-welded transverse attachment. The weld does not carry any load, and thus it can be categorized as an accessory weld. The used material is a UHSS with commercial name Strenx 1100 Plus (SSAB 2020). Three specimen batches were manufactured, to represent three different restraint conditions (Figure 13):

- 1) Unconstrained: the attachment was welded on a small plate specimen which was allowed to deform freely during welding and cooling.
- 2) Fixed: the attachment was welded on a similar specimen, which was clamped on the flange of a stiff I-beam during welding and cooling, to constrain both in-plane displacements and angular distortion.
- 3) Semi-rigid: the attachment was welded on a box beam flange, the box beam having remarkably lower bending stiffness than the I-beam of case 2.

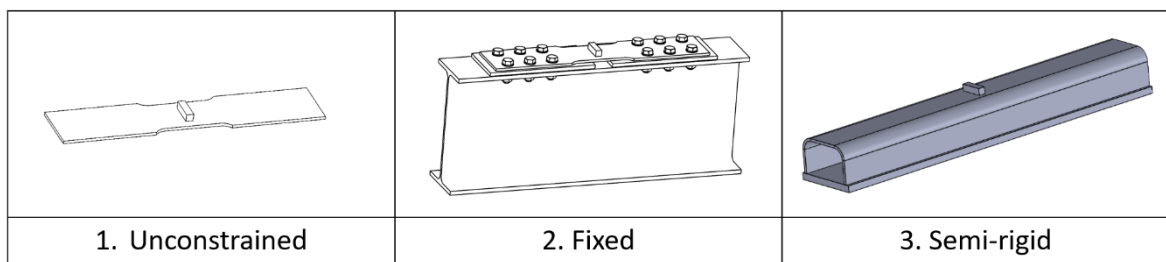


Figure 13. Constraint cases.

The stiffness properties of the structures in the different batches are listed in Table 2. The percentages show how much deformation has been prevented in relation to batch 1. The most significant differences between batches lie in axial stiffness; in batches 2 and 3, the bending stiffnesses are so high that practically all bending deformation is prevented in both cases.

Table 2. Stiffness properties of the welded specimens.

Batch	Cross section	Axial stiffness [kN/mm]	Bending stiffness [kNmm ²]	% of axial contraction prevented	% of angular distortion prevented
1	Plate specimen	574	1.0	0 %	0 %
2	IPE 400 & specimen	6 250	63 500	70.5 %	99.9 %
3	Box beam	4 080	3 060	40.1 %	99.3 %

In the calculation of the prevention of axial contraction, the effects of both axial stiffness and bending stiffness have been taken into account. For batches 1 and 2, the measured values of the welding distortions were obtained from the laboratory tests. The transverse weld shrinkage force was calculated from the measured axial contraction of the welded specimens (see chapter 7.2). After that, the axial contraction at specimen surface *due to membrane force* was calculated for batch 2 and 3 assemblies. Next, the axial contraction at specimen surface *due to bending moment* was calculated from the strain state at the specimen surface due to bending moment. Finally, the obtained total contraction was compared to the batch 1 axial contraction.

5.1.1 Batch 1: Unconstrained

Batch 1 demonstrates the case of a typical laboratory-scale specimen which has low geometrical stiffness, and the specimen itself provides little restraint upon welding deformations. The specimen is not clamped or otherwise attached, so that the deformations can occur freely. Hence, practically only tertiary and secondary residual stresses develop. The specimen of batch 1 is shown in Figure 14.

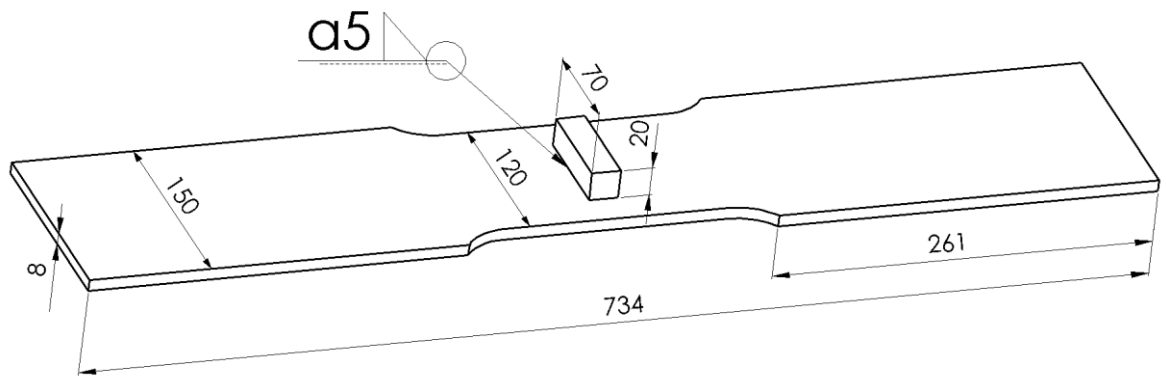


Figure 14. Test specimen for constraint cases 1 and 2.

Because the specimens were allowed to deform freely, rather large angular distortion occurs. If the distorted specimen were loaded in the fatigue test rig, disturbingly high bending stresses would occur due to the eccentricity of the load. To eliminate the angular distortion and these undesired bending stresses, pre-bending according to Figure 15 was made to batch 1 specimens before welding. Hence, a flat specimen geometry in as-welded condition was obtained: the measured average angular distortion after welding was only 0.3° .

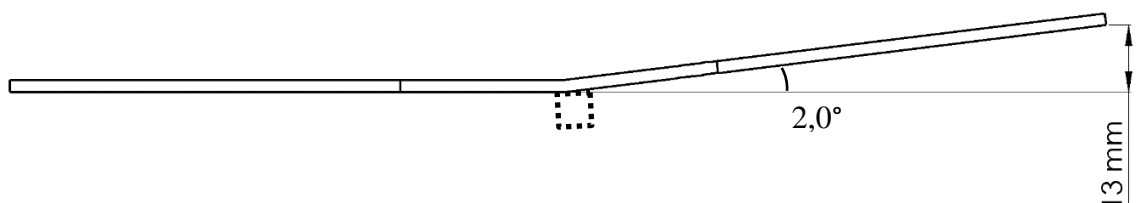


Figure 15. Pre-bending of batch 1 specimens.

5.1.2 Batch 2: Fixed

Batch 2 represents the case where the welded detail is a part of a stiff structure which provides high restraint. Hereby, same tertiary and secondary stresses are expected to develop as in batch 1, but in addition, high reaction forces will assumedly occur due to the support reactions caused by the surrounding stiff structure. These reaction forces cause primary reaction stresses to the specimen.

The specimens of batch 2 were otherwise identical to batch 1, except that bolt slots were cut to the plates of batch 2. Before welding, batch 2 specimens were bolted on an IPE 400 I-

beam (Figure 16). In this way, angular distortion was prevented, as well as most axial contraction.

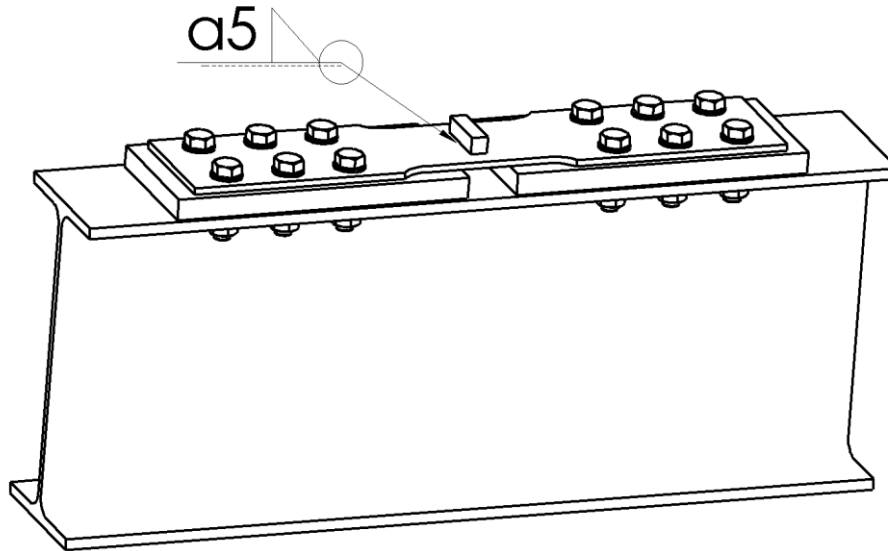


Figure 16. Constraint case 2.

The X-ray diffraction measurements of batch 2 were made after welding and cooling, while the specimen was still tightly clamped. Strain gauges were glued on the specimen surface. After this, the other bolt group was released so that the axial (membrane) contraction could take place. The bolts were tightened again, so that pure in-plane contraction could be measured by means of 3D-laser scanning. Finally, the specimen was entirely detached from the I-beam and 3D-scanned again, to measure also angular distortion. An additional X-ray residual stress measurement was made after de-clamping.

The specimen was installed in the test rig, and nominal loads identical to those of batch 1 were imposed. In addition, a pre-load force F_i was applied on top of the nominal loads, to reach same initial strain state as in the welded and still-clamped condition (Table 3). This simulates the situation that the detail is subjected to fatigue loads while still being attached to the stiff structure, where all primary reaction stresses are present.

5.1.3 Batch 3: Semi-rigid

Batch 3 represents the restraint case between batches 1 and 2, where the detail is a part of a moderately stiff structure. Hence, same tertiary and secondary residual stresses are expected to develop as in other batches, but lower primary stresses than in batch 2.

To create a semi-rigid condition, the same detail (transverse attachment) was welded on a box beam flange (Figure 17). For more detailed beam properties, see Appendix I.

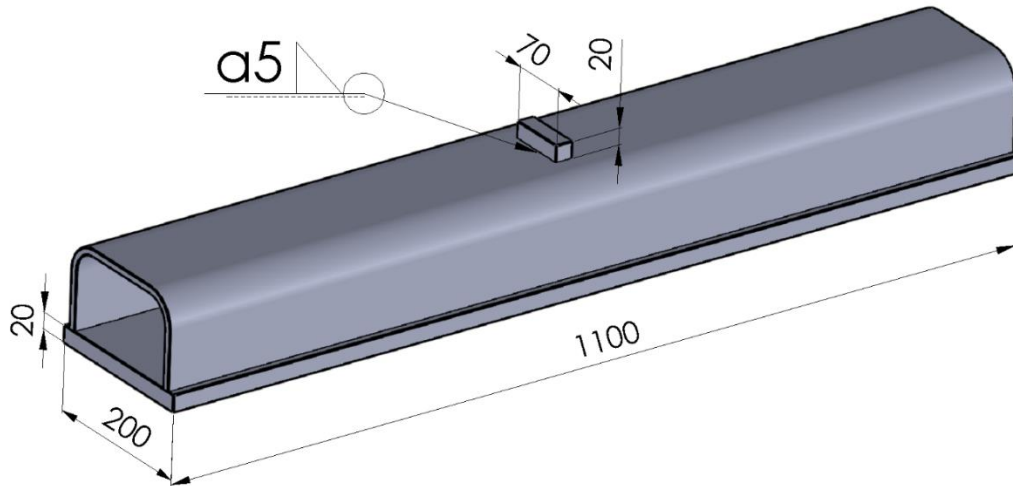


Figure 17. Constraint case 3.

In batch 3 box beams, the long attachment welds that connect the U-profile to the flange have been welded *after* the accessory weld. However, the attachment welds have little effect on the residual stress state in the opposite flange, because the beam cross section has been so designed that the arising membrane and bending components almost entirely neutralize each other.

5.1.4 Loads

All test specimens were subjected to alternating load to determine fatigue strength. For batches 1 and 2, tensile load was applied in a test rig (Figure 18).

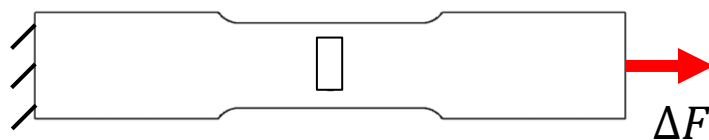


Figure 18. Loading setup of batches 1 and 2.

For batch 3, tensile stress to the flange was applied by means of four-point bending (Figure 19).

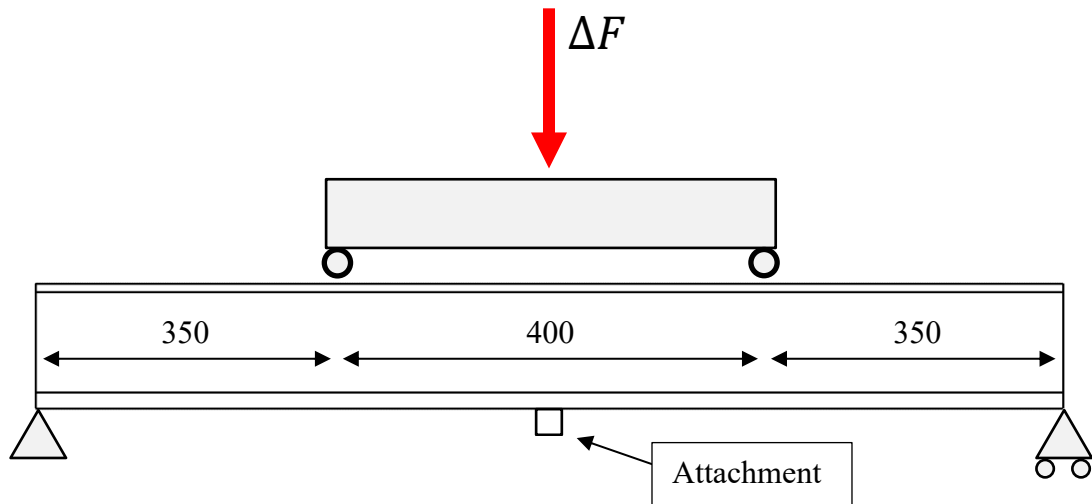


Figure 19. Four-point bending setup of batch 3.

Three nominal stress ranges ΔS (150, 180 and 260 MPa) and two stress ratios R (0.1 and 0.5) were used in different combinations, which are listed in Table 3. For batch 2, the pretension force $F_i = 130$ kN was applied in addition to the nominal load, to simulate the clamped and welded condition. The magnitude of F_i was determined by strain gauge measurements: as described in chapter 5.1.2, strain gauges were glued on batch 2 specimen surfaces prior to the loosening of the bolts. In the test rig, force was applied to achieve same strain state as in the clamped condition, and the applied force was measured. The nominal stress ranges in Table 3 are the intended values, not measured.

Table 3. Fatigue load parameters and test rig forces.

Batch / Specimen ID	ΔS [MPa]	R	ΔF [kN]	F_{\min} [kN]	F_{\max} [kN]
1. Unconstrained					
JS-1V1	150	0.1	144	16	160
JS-1V2	180		173	19	192
JS-1V3	260		250	28	277
JS-1V4	150	0.5	144	144	288
JS-1V5	180		173	173	346
JS-1V6	260		250	250	499

Table 3 continues. Fatigue load parameters and test rig forces.

Batch / Specimen ID	ΔS [MPa]	R	ΔF [kN]	F_{\min} [kN]	F_{\max} [kN]
2. Fixed					
JS-2V1	150	0.1	144	$16 + F_i$	$160 + F_i$
JS-2V2	180		173	$19 + F_i$	$192 + F_i$
JS-2V3	260		250	$28 + F_i$	$277 + F_i$
JS-2V4	150	0.5	144	$144 + F_i$	$288 + F_i$
JS-2V5	180		173	$173 + F_i$	$346 + F_i$
JS-2V6	260		250	$250 + F_i$	$499 + F_i$
3. Semi-rigid					
JS-P1	150	0.1	152	17	169
JS-P2	260		263	29	293
JS-P3	150	0.5	152	152	304
JS-P4	260		263	263	527

5.1.5 Materials and welding parameters

The base material of the specimens is SSAB's Strenx 1100 Plus. The chemical composition from the material certificate based on the steel manufacturer's ladle analysis is presented in Table 4.

Table 4. Chemical composition of Strenx 1100 Plus [weight-%].

C	Si	Mn	V	Cr	Ni	Mo	Ti	Al	Cu
0.132	0.196	1.49	0.154	1.35	1.01	0.402	0.014	0.046	0.459

Union X96 has been used as weld filler material. The mechanical properties of both Strenx 1100 Plus and Union X96 (Böhler Welding 2014) are listed in Table 5.

Table 5. Mechanical properties of materials.

Material	Proof strength $R_{p0.2}$ [MPa]	Ultimate strength [MPa]	Elongation at break [%]	Young's modulus [GPa]
Strenx 1100 Plus	1157	1188	14.3	204.5
Union X96	930	980	14.0	-

The attachments were welded with GMAW. The welding parameters are listed in Table 6. Heat input was calculated according to the standard EN 1011-1. The maximum heat input recommended by the steel manufacturer is 1.16 kJ/mm for Strenx 1100 Plus and 8 mm plate thickness.

Table 6. Welding parameters.

Batch	Voltage [V]	Current [A]	Travel speed [mm/s]	Heat input [kJ/mm]
Batch 1	27.3	218	4.0	1.19
Batch 2	27.0	217	4.0	1.17
Batch 3	27.5	217	4.0	1.19

As Table 6 indicates, the maximum recommended heat input was exceeded by 2.1 % in average. The recommended cooling time from 800 °C to 500 °C ($t_{8/5}$) of 5–15 seconds has been specified by the steel manufacturer. In these test specimen welds, the average $t_{8/5}$ time was 77.0 seconds, which implies that the cooling rate has been excessively slow.

5.1.6 Post weld treatment

Residual stresses, temperatures and strains were measured from one weld toe region only, and fatigue crack nucleation at this toe region was desired. Therefore, it was necessary to prevent crack nucleation elsewhere; the opposite weld toe was treated by high frequency mechanical impact (HFMI) treatment, to prevent undesired fatigue crack nucleation (Figure 20).

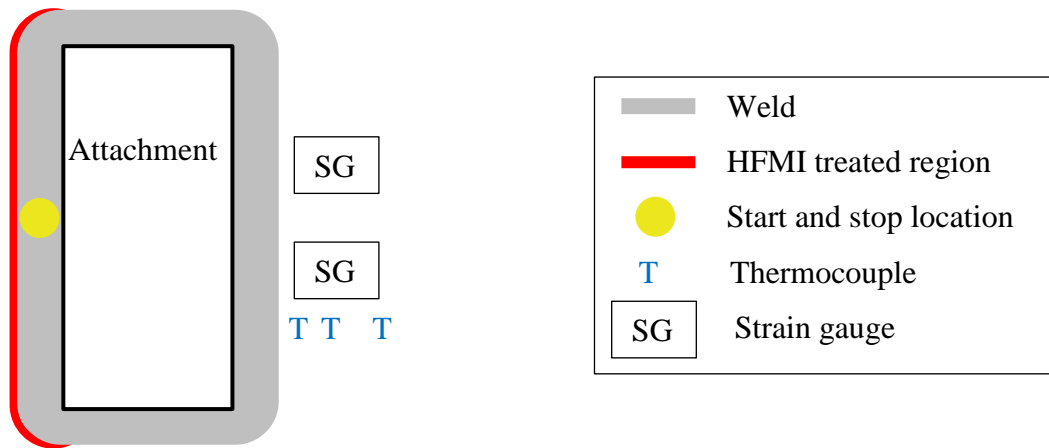


Figure 20. HFMI treated region.

5.2 Numerical analysis

The fatigue strength of the detail was assessed using two methods: nominal stress method and 4R method. The assessment procedures are shortly described in this chapter.

5.2.1 Secondary bending

Prior to the fatigue strength assessment, the degree of secondary bending was determined by analytical calculations. Batch 1 and 2 specimens are tension loaded, and hence the secondary bending stress σ_b due to axial load and angular distortion is calculated from:

$$\sigma_b = S \cdot \frac{bt \frac{L}{2} \sin\left(\frac{\alpha_d}{2}\right)}{\frac{bt^2}{6}} \quad (11)$$

where L is clamping length, S is applied nominal membrane stress, and α_d is distortion angle (Figure 21). Plate width b is reduced from the equation. The clamping length L equals to 230 mm for both batches. The values of α_d have been measured by means of laser scanning.

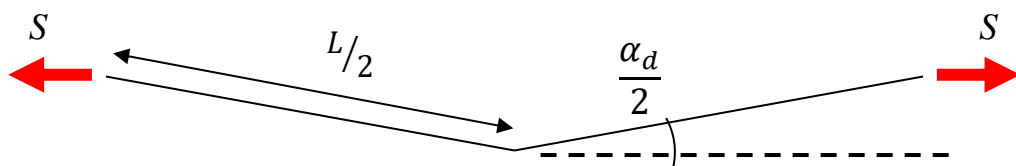


Figure 21. Determination of secondary bending.

Batch 3 specimens are bending loaded. In the tension (bottom) flange of the box beam, the global bending moment produces normal stress distribution as shown in Figure 22.

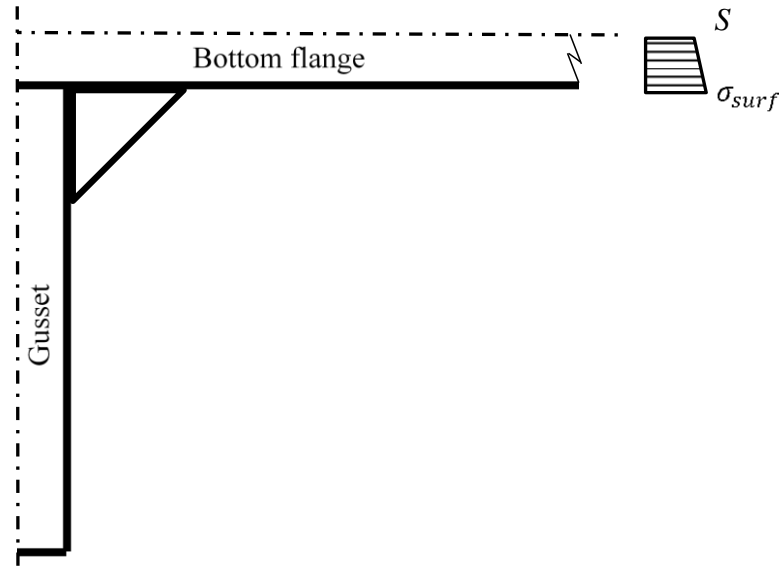


Figure 22. Normal stress distribution in box beam flange.

The bending stress σ_b in the flange is calculated from

$$\sigma_b = \sigma_{surf} - S \quad (12)$$

where σ_{surf} is the nominal surface stress. The formulas for σ_{surf} and S substituted, equation 12 is reduced to

$$\sigma_b = S \cdot \frac{t}{2y_m} \quad (13)$$

where t is flange plate thickness, and y_m is the distance between box beam neutral axis and flange mid-plane. The values of both angular distortion and σ_b are listed in Table 7.

Table 7. Secondary bending stresses due to angular misalignment and membrane load.

Batch	α_d	σ_b
1	0.3°	0.23·S
2	0.8°	0.60·S
3	-	0.05·S

5.2.2 Evaluation with nominal stress method

The fatigue life of the welded detail was first assessed using the nominal stress method. In this method, the fatigue life N_f of the detail is calculated from (Hobbacher 2008, p. 99):

$$N_f = \left(\frac{\text{FAT}}{k_{m,eff} \cdot \Delta S} \right)^m \cdot 2 \cdot 10^6 \quad (14)$$

where FAT is the fatigue class of the detail category of nominal stress method, m is the slope of the S-N curve, ΔS is the nominal stress range in the structure, and $k_{m,eff}$ is the effective stress magnification factor which accounts for joint misalignment. For this particular detail, FAT = 71 MPa and $m = 3$ are selected (Figure 23).

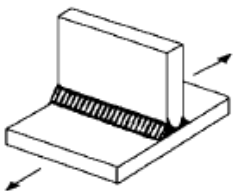
500	Non-load-carrying attachments			
511		Transverse non-load-carrying attachment, not thicker than main plate K-butt weld, toe ground Two sided fillets, toe ground Fillet weld(s), as welded thicker than main plate	 100 100 80 71	 36 36 28 25

Figure 23. Nominal FAT class of the weld (Hobbacher 2008, p.64).

As equation 14 shows, the nominal fatigue class is reduced by a stress magnification factor. The calculated stress magnification factors $k_{m,calc}$ were determined by formula (Mod. Hobbacher 2008, p. 99–100):

$$k_{m,calc} = \frac{\sigma_{surf}}{\sigma_m} = \frac{S + \sigma_b}{S} \quad (15)$$

where σ_{surf} is the total stress at plain plate surface when the effects of secondary bending have been taken into account, and σ_m is the applied nominal membrane stress. According to Hobbacher (2008, p. 100), stress magnification factor of 1.25 has already been covered in the FAT class of the detail and thus, effective stress magnification factor $k_{m,eff}$ should be used. The factor $k_{m,eff}$ is calculated from (Hobbacher 2008, p. 99):

$$k_{m,eff} = \frac{k_{m,calc}}{k_{m,cov}} \quad (16)$$

where $k_{m,calc}$ is the calculated stress magnification factor, and $k_{m,cov}$ is the stress magnification factor already covered in the FAT class. In this study, effective stress magnification factors smaller than one were rounded to one. The obtained factors are tabulated in Table 8. In the table, effective fatigue class FAT_{eff} is FAT divided by $k_{m,eff}$.

Table 8. Stress magnification factors of nominal stress method.

Batch	$k_{m,calc}$	$k_{m,cov}$	$k_{m,eff}$	FAT_{eff}
1	1.23	1.25	1	71
2	1.60	1.25	1.28	55
3	1.05	1.25	1	71

5.2.3 Evaluation with 4R method

The 4R formula for fatigue life evaluation has already been presented in chapter 2.6.2. The values of the effective notch stress range $\Delta\sigma_k$ were calculated using the SCFs received from the FEA (chapter 5.2.4), and the applied nominal stress ranges (chapter 5.1.4). The input parameters which are common to all batches are listed in Table 9. Sharp toe (radius of 0 mm) was assumed. To achieve a worst-case assessment, the highest measured residual stress value from each batch was used, according to the higher scatter band of the measurements.

Table 9. 4R parameters.

Parameter	Symbol	Value	Unit
Young's modulus	E	204 500	MPa
Ultimate strength	R_m	1 188	MPa
Proof stress	$R_{p0,2}$	1 157	MPa
Plasticity modulus	H	1 960	MPa
Strain hardening exponent	n	0.15	-
Characteristic fatigue capacity	C_{char}	$10^{20.83}$	-
Mean fatigue capacity	C_{mean}	$10^{21.59}$	-

Table 9 continues. 4R parameters.

Parameter	Symbol	Value	Unit
Slope of master curve	m_{ref}	5.85	-
Actual toe radius	r_{true}	0	mm

5.2.4 FEA

Structural and notch stress concentration factors (SCFs) were obtained from linear static finite element analysis (FEA). Linear elastic material model was used. Firstly, the structural stress redistribution effect caused by the attachment was analyzed with a simplified 3D solid element model. The hot spot stress at the weld toe was determined, and two geometries were compared with each other (Figure 24): The actual structure with 70 mm wide attachment (3D-case), and a structure which is continuous in the Y-direction (2D-case). Due to the structural effect, stresses in the 3D-case were higher: 6 % higher stress was observed with membrane load, and 11 % higher stress with bending load. Thus, structural stress concentration factor for membrane load $k_{s,m} = 1.06$ and structural stress concentration factor for bending load $k_{s,b} = 1.11$ were obtained.

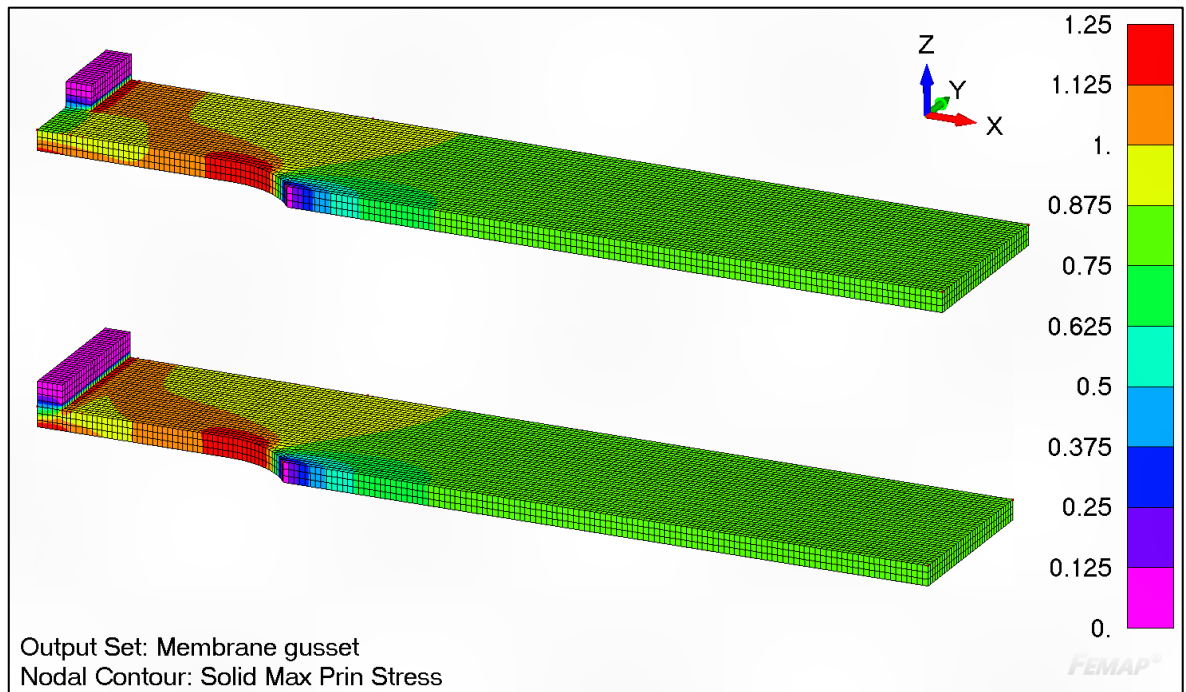


Figure 24. 3D FE model.

Secondly, a 2D-representation of the detail geometry was modelled according to the real geometry of the weld (Appendix II) and 1 mm rounding at the toe, to determine effective notch stress factors. Linear plate elements with plane strain formulation were used (Figure 25).

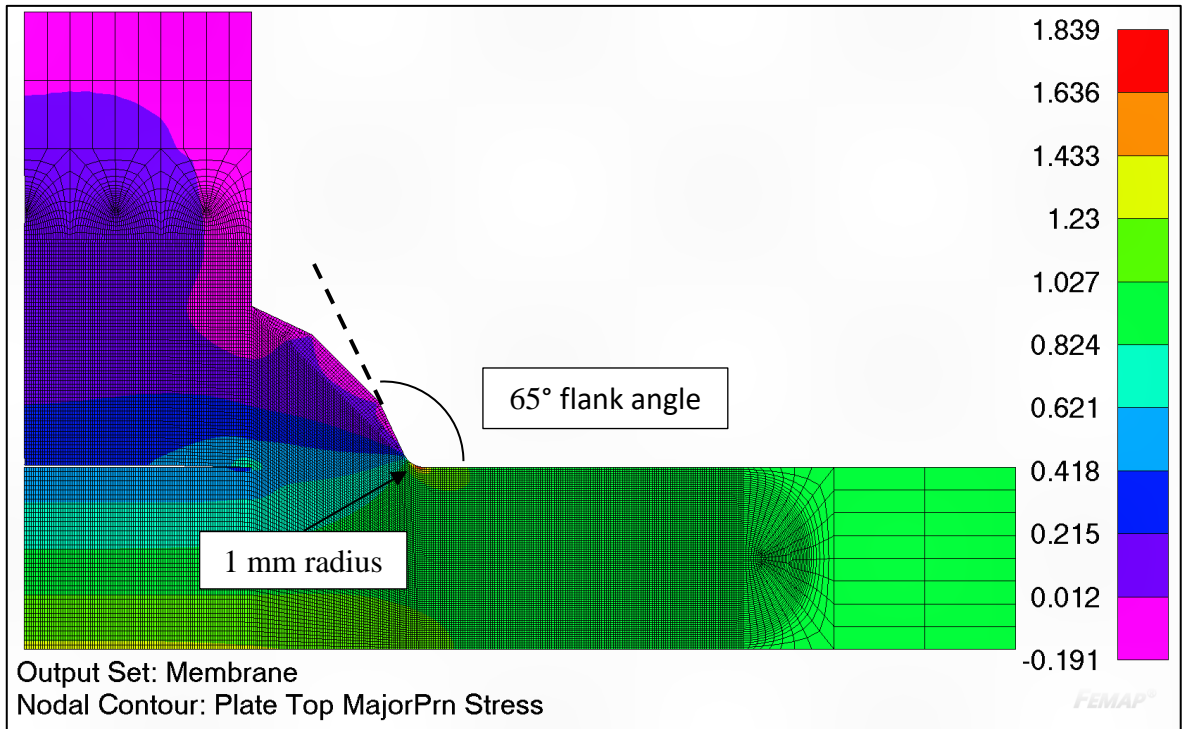


Figure 25. 2D FE model.

Both membrane and bending notch stress factors were determined using 1 MPa nominal load. Membrane load of 1 MPa produces 1.839 MPa notch stress. Thus, membrane notch stress factor $k_{t,m} = 1.839$ was obtained. Similarly, 1 MPa bending load produces 2.202 MPa stress, whence bending notch stress factor $k_{t,b} = 2.202$ was obtained. Now, the effective notch stress range $\Delta\sigma_k$ can be calculated for each nominal stress range ΔS :

$$\Delta\sigma_k = \Delta S \cdot k_{s,m} \cdot k_{t,m} + \Delta\sigma_b \cdot k_{s,b} \cdot k_{t,b} \quad (17)$$

Values of $\Delta\sigma_b$ are obtained from ΔS using the coefficients from Table 7. The calculated effective notch stresses for different batches are listed in Table 10. The nominal stress ranges in Table 10 are actual measured values from the tests.

Table 10. Effective notch stress ranges due to measured nominal stresses.

Batch / Specimen ID	ΔS [MPa]	R	$\Delta\sigma_b$ [MPa]	$\Delta\sigma_k$ [MPa]
1. Unconstrained				
JS-1V1	151	0.1	34	378
JS-1V2	181		41	453
JS-1V3	259		58	648
JS-1V4	151	0.5	34	378
JS-1V5	180		41	450
JS-1V6	259		58	648
2. Fixed				
JS-2V1	151	0.1	91	517
JS-2V2	181		109	619
JS-2V3	260		157	889
JS-2V4	151	0.5	91	517
JS-2V5	181		109	619
JS-2V6	259		156	886
3. Semi-rigid				
JS-P1	151	0.1	8	313
JS-P2	260		13	538
JS-P3	154	0.5	8	319
JS-P4	263		13	545

As Table 10 indicates, batch 2 has higher effective notch stresses compared to batch 1. This is due to the effects of secondary bending, which are most pronounced in heavily distorted specimens. Batch 3 exhibits lowest notch stresses, due to low secondary bending.

6 RESULTS

In this chapter, the results of experimental testing are presented. The results consist of temperature, deformation, residual stress and fatigue test results.

6.1 Temperature history

The temperature history during welding and cooling was measured with thermocouples, which were placed at locations shown in Figure 26. In addition, the temperatures at the middle of the weld were measured with a pyrometer. The temperature history results of specimen “JS-P2” are illustrated in Figure 27. The temperature curves of other specimens are similar to the presented one.

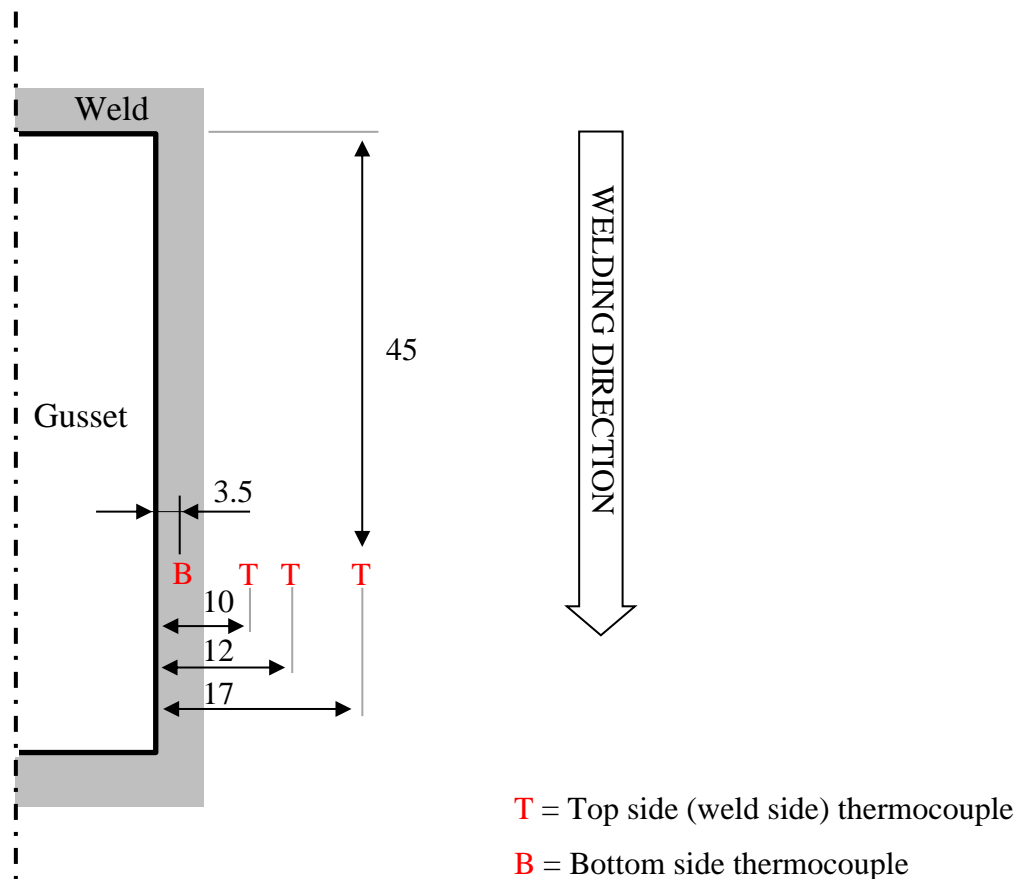


Figure 26. Temperature measuring points.

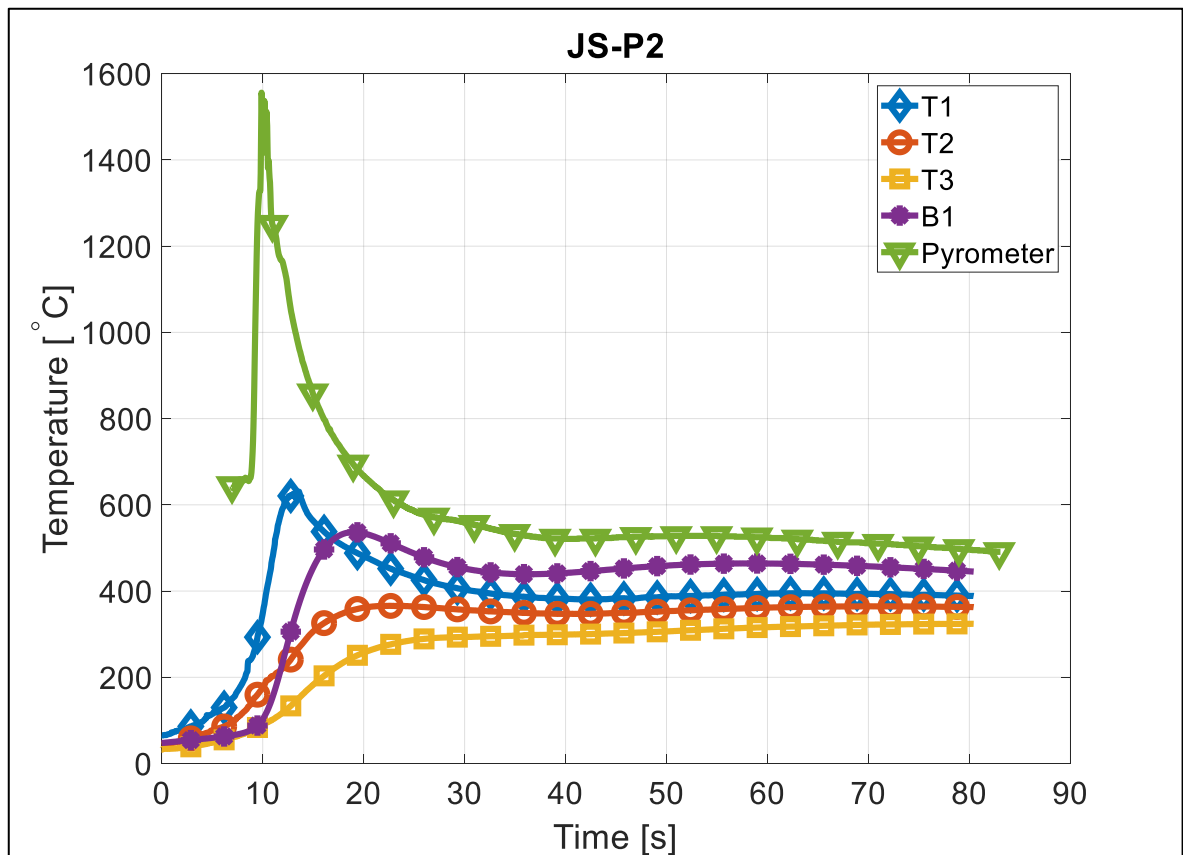


Figure 27. Temperature history of specimen "JS-P2".

6.2 Welding deformations

Angular distortions of the test specimens of batches 1–2 were measured with 2D- and 3D-laser scanning. In batch 2, also axial contraction was measured. The measured welding distortions (average values) are listed in Table 11.

Table 11. Average welding distortions.

Batch	Angular distortion	Axial contraction
1	0.3°	-
2	0.8°	0.091 mm

In batch 1 specimens, rather straight geometry was obtained. Also batch 2 specimens, which were welded in clamped condition, show only moderate angular distortion.

6.3 Residual stresses

To determine the surface residual stress profiles in the vicinity of the weld toe, the transverse residual stresses (normal stress in x-direction, Figure 28) were measured with X-ray diffractometer.

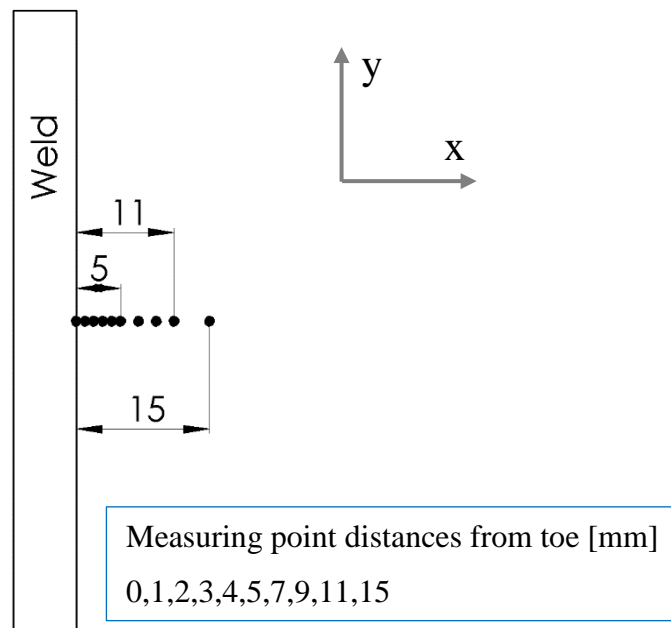


Figure 28. X-ray measurement locations. Stress in X-direction was measured.

The full residual stress profile was measured from one specimen in each batch. The stress at weld toe was measured from all specimens. The average residual stresses at the weld toes are listed in Table 12.

Table 12. Average residual stresses at weld toes.

Batch	Average σ_{res} at toe
1	115 MPa
2	676 MPa
3	-123 MPa

The surface residual stress profiles are plotted in Figure 29. The stresses of batch 2 have been measured in the clamped condition.

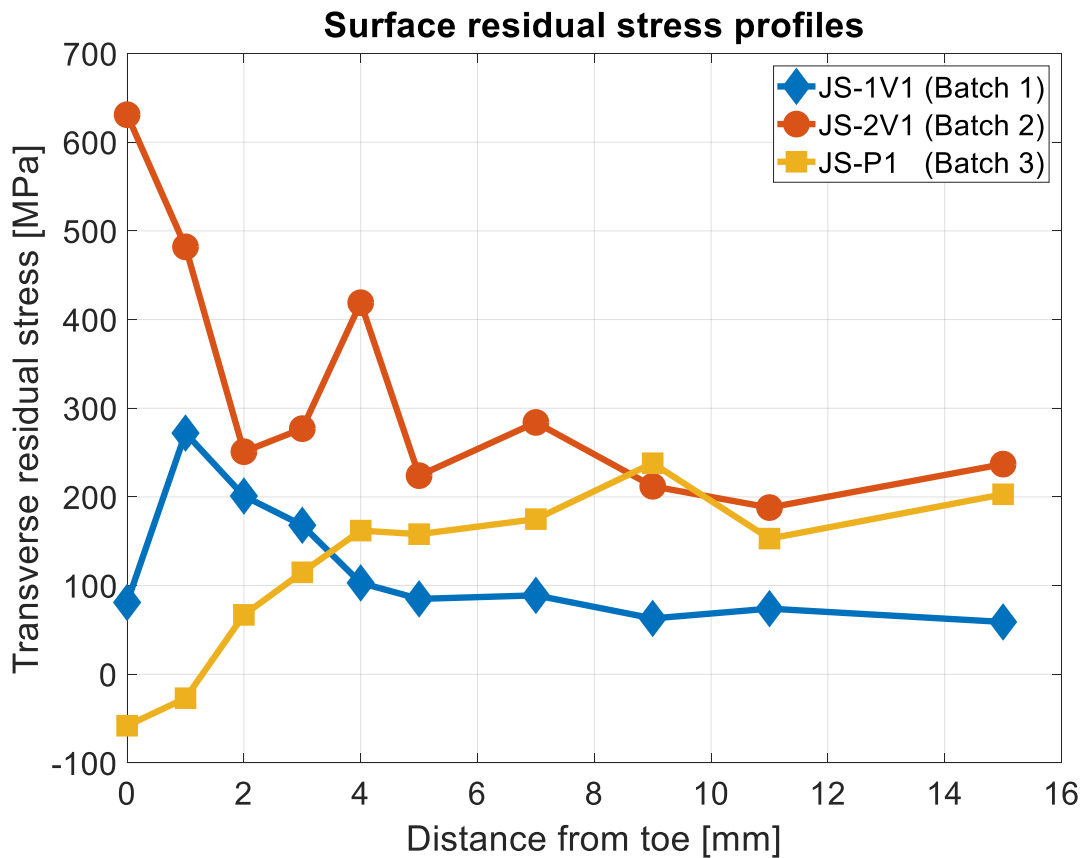


Figure 29. Surface transverse residual stress profiles.

In the profile of batch 1 specimen, tensile residual stress has been observed at all regions. The highest tensile stress is not found in the toe region, but at 1–2 mm distance from the toe. This is in good accordance with the findings of Hensel et al. (2015) reported in chapter 3.6.

The profile of batch 2 specimen lies in general approximately 150 MPa higher than batch 1 specimen, that is, a shift upwards (to higher tensile stress) can be observed. This is supposedly caused by the primary reaction stresses due to restraint, which are superpositioned upon the secondary and tertiary stresses which develop in a freely deformed specimen. However, at the weld toe and its close vicinity, the batch 2 curve shows a sharp stress peak, having approximately 550 MPa higher tensile stress at the toe than the freely deformed specimen. This could be explained so that the notch effect of the weld would give local raise to the primary residual stresses. Yet, this contradicts the findings of Farajian et al. (2014) reported in chapter 3.6, where a parallel shift upwards was observed also in the toe region (Figure 5).

The profile of batch 3 specimen shows compressive residual stress at the weld toe and its close vicinity. A rising trend can be noted when moving further from the toe, and at 7–8 mm and longer distances from the toe, the stress profile can be regarded identical to that of batch 2. The compressive stress at the toe is unexpected: on the contrary, higher tensile residual stresses than in freely deformed specimens would have been expected, due to the primary residual stresses which are created by the restraint from the geometrical stiffness of the beam.

The compressive stress state at the toe can be partly explained by the HFMI treatment. The HFMI treatment of batch 1 and 2 specimens was made after the residual stress measurements, and thus the measurements correctly show the residual stress state in the as-welded state. However, to batch 3 specimens the HFMI treatment was unintentionally made *before* the residual stress measurements. This was a clear mistake in the test setup. Although the HFMI treatment was made to the opposite toe (Figure 20), it clearly affects also the measured toe, as shown in Figure 30. Gauge 1 was glued at 3.2 mm distance from the measured toe (Figure 20).

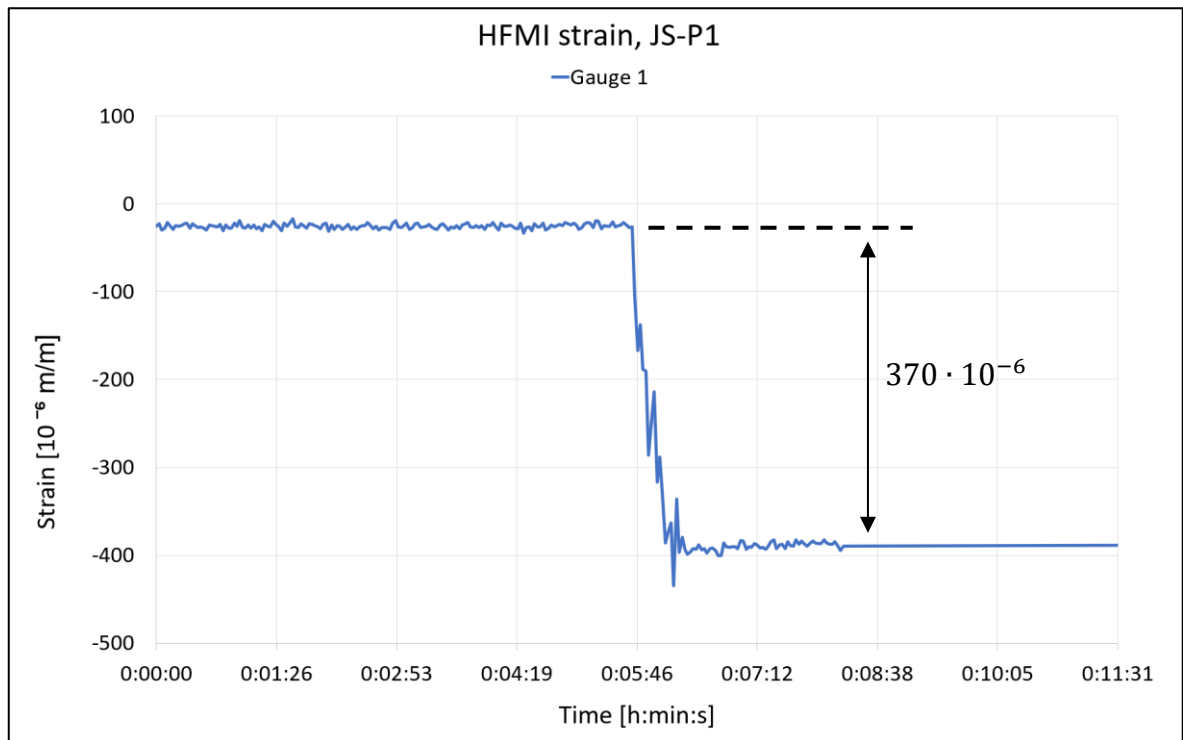


Figure 30. Strain at 3.2 mm distance from toe, before and after HFMI.

As a consequence of the HFMI treatment, the strain at the measuring point (3.2 mm from the toe) decreases approximately 370 microstrains, which corresponds to 78 MPa in normal stress. This is supposedly multiplied by the notch effect of the weld so that the local decrease at the toe can be more than 100 MPa. Due to this effect, the measured residual stress profiles of batch 3 specimens are not directly comparable to the others.

In Figure 31, the residual stress profile of a batch 2 specimen is presented in both clamped and released condition. In addition, the curve of the batch 1 specimen is plotted for comparison.

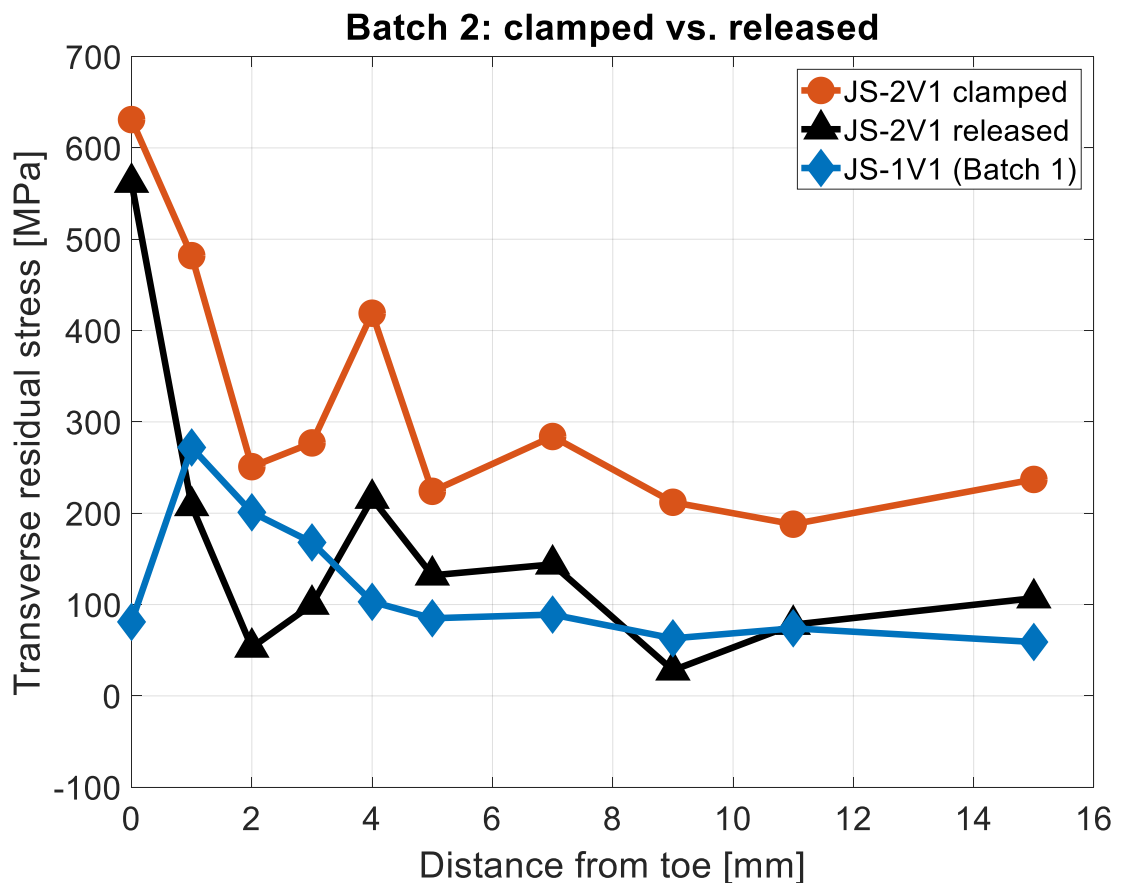


Figure 31. Effect of releasing the clamp in batch 2.

An average decrease of 160 MPa in residual stress is observed as a consequence of the clamp release. In general, this decrease brings the batch 2 curve to the same level with the batch 1 curve. The weld toe is a remarkable exception: In the weld toe of the de-clamped batch 2 specimen, approximately 500 MPa higher residual stress is found than in the batch 1 specimen. This contradicts the findings of Schroepfer & Kannengiesser (2014), who

observed a decrease of approximately 250 MPa in tensile residual stress at the toe, when going from the freely welded specimen to the de-clamped one. In other words, the freely welded specimen showed higher toe stress than the restrained and de-clamped specimen. Though, the test setups of Schroepfer & Kannengiesser (2014) and this thesis differ in that Schroepfer & Kannengiesser have researched butt welds (Figure 6), which have lower notch effect than the fillet welds of this work.

As Figure 31 shows, the primary reaction stress is approximately 160 MPa. At the weld toe, the notch effect of the weld should give a significant local raise to this stress. However, according to the measurement results, only 100 MPa stress decrease is observed at the toe. In X-ray residual stress measurements, the scatter of the results can be tens of megapascals, and this difference between toe and surroundings can possibly be explained by measurement inaccuracy. Yet, measurement inaccuracy alone cannot explain why the residual stress in the de-clamped batch 2 specimen is so much higher than in batch 1. Primary residual stresses equilibrate with the support reactions only, and therefore they relax completely when the support reactions are removed. Thus, it is obvious that higher secondary and/or tertiary stresses have developed in the batch 2 specimen due to the clamped condition during welding.

6.4 Fatigue lives

The results of the fatigue tests are listed in Table 13, together with the measured nominal stress ranges, applied stress ratios and the calculated characteristic fatigue classes (FAT_{char}).

Table 13. Fatigue test results.

Batch, Specimen ID	ΔS [MPa]	R	Fatigue life [cycles]	FAT _{char} [MPa] m=3
1. Unconstrained				
JS-1V1	151	0.1	360 489	63
JS-1V2	181		197 496	
JS-1V3	259		89 278	
JS-1V4	151	0.5	186 284	52
JS-1V5	180		125 798	
JS-1V6	259		44 439	
2. Fixed				
JS-2V1	151	0.1	188 368	51
JS-2V2	181		117 673	
JS-2V3	260		43 266	
JS-2V4	151	0.5	246 570	51
JS-2V5	181		93 804	
JS-2V6	259		38 545	
3. Semi-rigid				
JS-P1	151	0.1	220 739	55
JS-P2	260		43 809	
JS-P3	154	0.5	156 867	51
JS-P4	263		32 151	

The fatigue lives are illustrated with a bar graph in Figure 32. It can be noted that the fatigue life is shortened by the welding restraint: The freely deformed specimens (batch 1) have longest fatigue lives, and the specimens with fixed boundary condition (batch 2) have the shortest. The results of the semi-rigid case (batch 3) lie between these extremes.

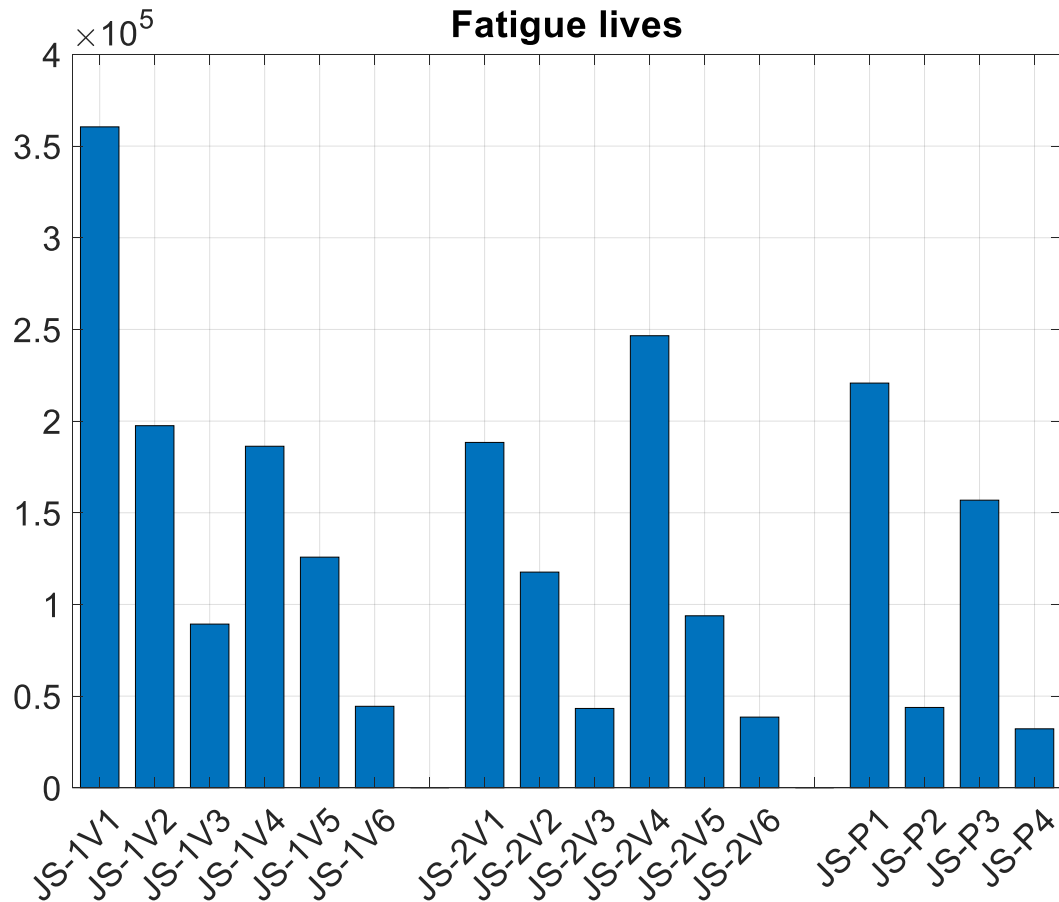


Figure 32. Fatigue lives.

The mean fatigue lives with survival probability $P_s = 50\%$ were calculated using two assessment methods: nominal stress method and 4R method. In the nominal stress method calculations, characteristic fatigue class (FAT) of 71 MPa was used (Hobbacher 2008, p. 64). The effective stress magnification factors were used (chapter 5.2.2). The mean fatigue class ($P_s = 50\%$) was obtained by multiplying the characteristic design fatigue class by the factor of 1.37 (Sonsino 2012, p. 7).

Also the characteristic fatigue lives ($P_s = 97.7\%$) were calculated with both methods. The calculated fatigue lives were divided by the actual fatigue lives received from the tests. Hence, percentage values were obtained to describe the relative differences of the calculated and actual values. The percentages are plotted in Figure 33 and Figure 34.

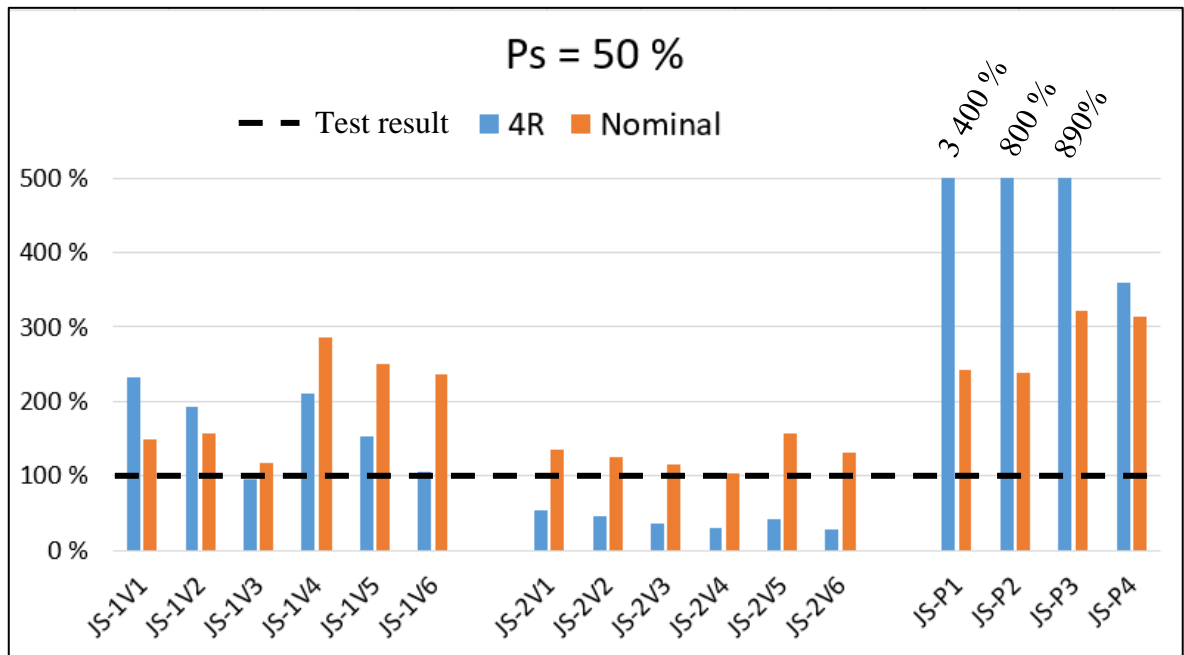


Figure 33. Calculated mean fatigue lives ($P_s = 50\%$) in relation to the test results.

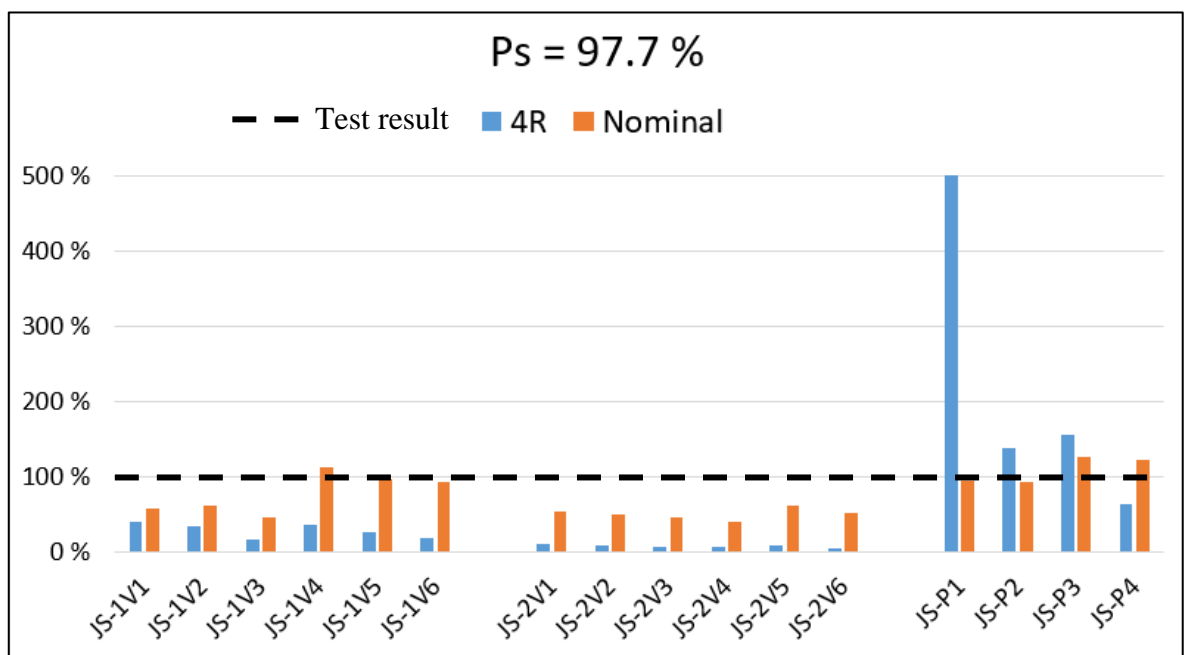


Figure 34. Calculated characteristic fatigue lives ($P_s = 97.7\%$) in relation to test results.

With the nominal stress method, it can be observed that with low restraint and low stress ratio $R = 0.1$, there is rather good agreement between the test results and the numerical assessments. When higher stress ratio $R = 0.5$ is used or when the specimens are welded

under higher restraint, the method gives either too pessimistic or clearly non-conservative results.

With the 4R method, the results are rather accurate when the welding restraint is low. However, with highest welding restraint (batch 2) where the tensile residual stresses are highest, the results appear overly conservative. With batch 3, the results are pronouncedly non-conservative. The reason for the optimistic 4R predictions is most probably the compressive residual stress state of the batch 3 specimens. However, this favourable effect of the compressive stress seems to be absent from the actual test results.

6.5 S-N curves

S-N curves have been derived from the fatigue test results. Fixed slope $m = 3$ has been used in the curve fitting. The mean (50 % survival probability) S-N curves for nominal stress approach are plotted in Figure 35. In the figure legend, B1=batch 1, B2=batch 2, etc.

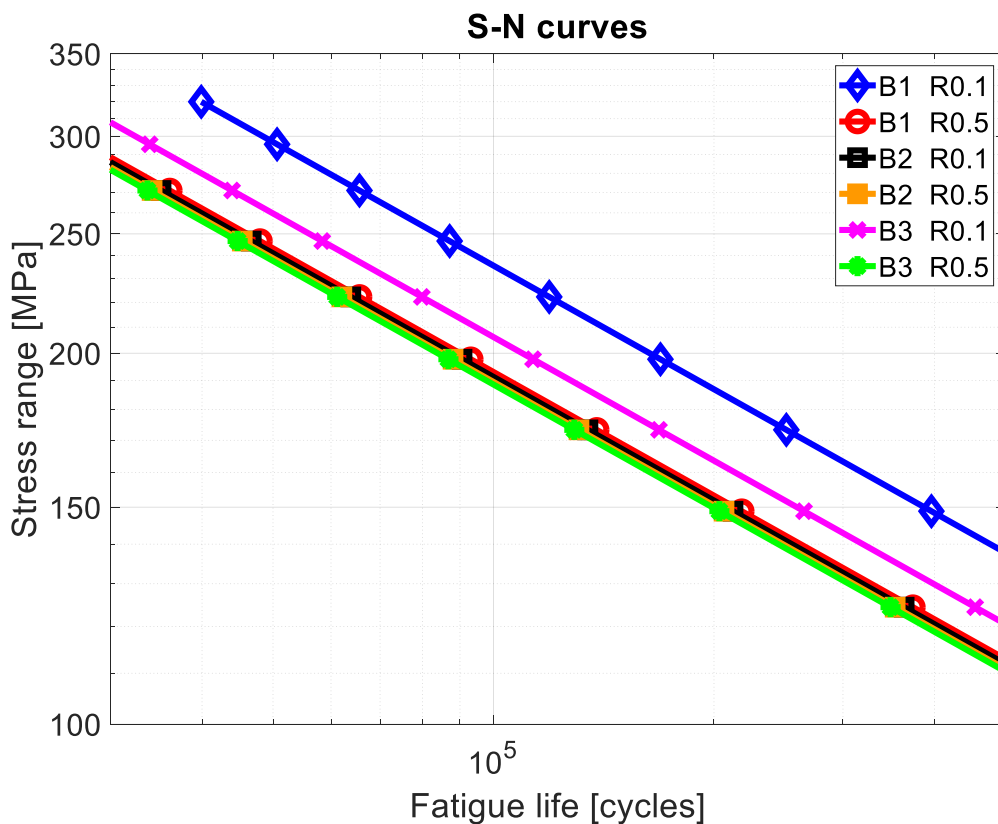


Figure 35. Mean S-N curves, nominal stress approach. Survival probability 50 %.

Nominal mean FATs with survival probability $P_s = 50\%$ are obtained from the S-N curves. The fatigue classes are illustrated with a bar graph in Figure 36.

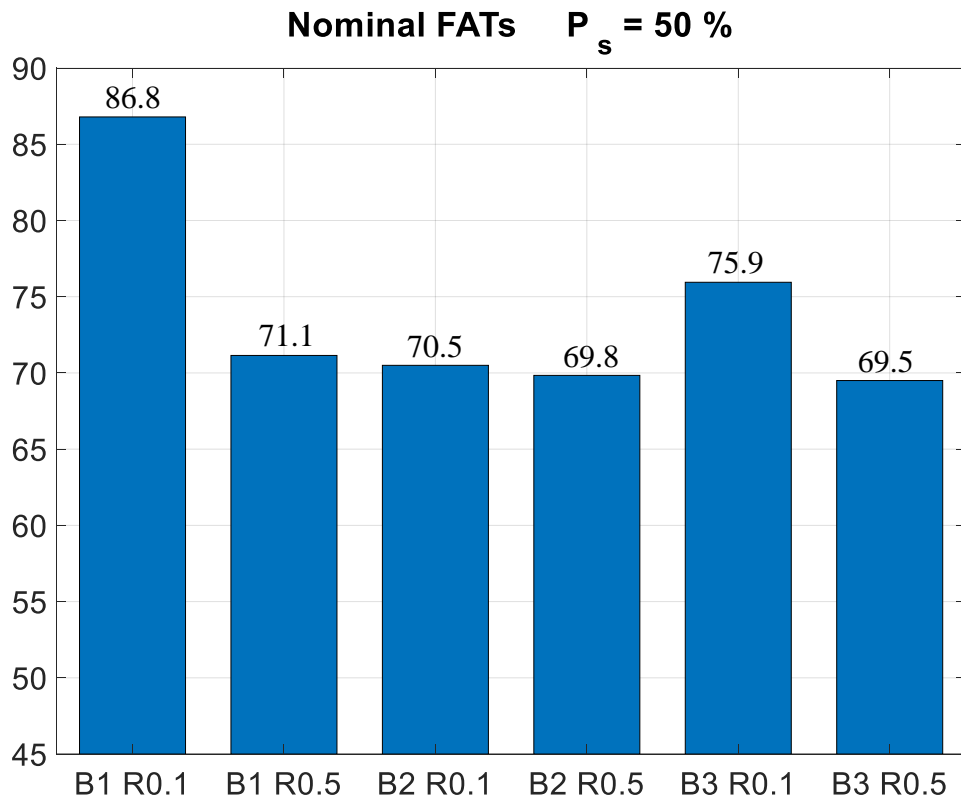


Figure 36. Mean FAT classes, survival probability 50 %.

Due to the low number of test specimens, Characteristic FAT classes could not be derived from the standard deviation of the test data. Instead, characteristic FAT classes with 97.7 % survival probability were derived from the mean FATs by division by the factor of 1.37 (Sonsino 2012, p. 7). The characteristic FAT classes are plotted in Figure 37.

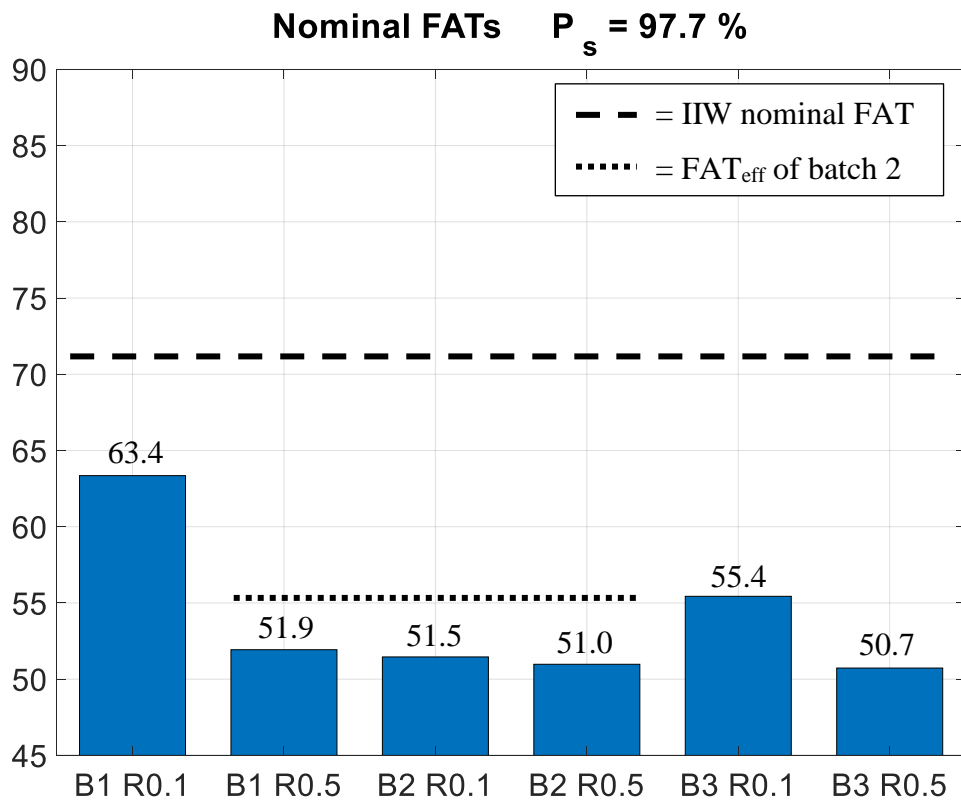


Figure 37. Design FAT classes, survival probability 97.7 %.

As it can be observed, the obtained characteristic FATs are relatively low. For comparison, IIW recommendations give design FAT class of 71 MPa to this structural detail. The low fatigue resistance of the specimens could be partly explained by the softening of the material in the HAZ. Though, the hardness measurements (Appendix II) do not show any remarkable softening. Another possible reason is the rather steep flank angle of the weld (65° in average).

7 DISCUSSION

Analytical discussion about the experimental tests and test results is provided in this chapter. Firstly, additional test result analysis is given, to complement the discussion in chapter 6. Secondly, a self-critical look is taken into the test setup, to reveal any flaws that might affect the conclusions.

7.1 Analysis of results

The long $t_{8/5}$ times imply excessively low cooling rates which, according to Schroepfer & Kannengiesser (2014), predict high primary residual stresses and short fatigue life. The residual stresses are indeed high, especially in the clamped specimens: 160 MPa residual stress increase was observed as a consequence of fixed welding boundary condition. This stress relaxed after releasing the clamp. However, after de-clamping, 500 MPa higher residual stress still remained at the toe of the de-clamped specimens, compared to the freely deformed specimens. Thus, it can be concluded that the fixed boundary condition causes general residual stress raise due to the primary residual stress, but also gives – somewhat surprisingly – a considerable increase to the secondary and tertiary stresses at the toe. No notch effect could be observed to give raise to the primary residual stresses.

Judging by the strain gauge results, the crack propagation life dominated: typically, $\frac{2}{3}$ of the total fatigue life consisted of crack propagation, and the crack nucleation times remained relatively short. This suggests poor weld quality in terms of steep flank angle and sharp toe radius. No undercuts were observed at the critical weld toes.

The fatigue lives were unexpectedly short: the calculated design FATs range between 51–63 MPa, whereas the design FAT given by Hobbacher (2008) is 71 MPa, and hence the strongest specimen was 11.3 % weaker than predicted by Hobbacher (2008). The weak fatigue resistance of the test specimens could be partly explained by poor weld geometry: the flank angles were 65° in average. The excessively slow cooling rate could possibly predict softening in the HAZ, which could lead to weakened fatigue resistance. Yet, the hardness measurements do not confirm any significant softening.

In general, it can be stated that the welding boundary conditions have a clear effect on the fatigue strength of an accessory weld. The stiffer the boundary condition, the weaker the structure: a 1 000 % increase in axial stiffness results in a 18 % decrease in fatigue strength. The specimens of low restraint show some mean stress dependence, but in the high restraint specimens, no notable mean stress effect can be found.

7.2 Test arrangement shortcomings

In the fatigue tests of batch 2, the clamped condition was simulated in the test rig. The intention was to produce the same deformation state in the test rig as was in the clamped condition, as if the specimen were a part of a stiffer structure also during the fatigue loading. In practice this means that the primary reaction stresses have to be present all the time. This was accomplished by applying initial load F_i , to compensate the axial contraction which had occurred in de-clamping. (Chapter 5.1.2). The problem with this approach is that it does not accurately mirror the reality: In reality, the reaction stresses are displacement-controlled; although these stresses do not practically relax due to local notch yielding, some relaxation nevertheless occurs due to crack propagation. Therefore, the restraint stresses do not fully contribute to the final fracture, due to the relaxation behavior. In the test, F_i is a force-controlled load which *does* contribute to the final fracture. Therefore, final fracture occurs too soon in the test, and the test gives slightly lower fatigue life than is expected in reality, that is, the results become somewhat over-conservative. In addition, as shown by Farajian et al. (2014), tensile residual stress relaxation due to initial load is also more pronounced with stiff specimens. This has not been accounted for in the test setup, and therefore, overly pessimistic results may have been achieved for the impact of primary stresses.

Another problem with batch 2 is that an overly large F_i had to be used to reach same surface strain state in the test rig as was in the clamp. This occurred because the strain at the plate surface in the clamped condition is caused by both membrane and bending load, and bending load could not be applied in the test rig. Therefore, the lack of bending needed to be compensated by overly large membrane load F_i . This has assumedly little effect on crack nucleation, but might shorten the crack propagation life. This phenomenon introduces even more conservativity into the batch 2 results.

As discussed before in chapter 6.3, the HFMI treatment of the batch 3 specimens was accidentally made prior to the residual stress measurements. For this reason, no residual stress profile of batch 3 could be obtained in the as-welded state. This makes it difficult to draw conclusions on the magnitude of the primary residual stress after welding, and its effect on the fatigue life. Since the residual stress profiles of the other batches were measured prior to the HFMI, also comparison between the residual stress profiles of batch 3 and other batches is hardly meaningful. The same pertains to the comparison of the 4R results, since the residual stress state at the weld toe is one input parameter of the 4R calculation formulae.

8 CONCLUSIONS

The effect of welding boundary conditions on the residual stress state and fatigue strength of a non-load-carrying accessory joint was studied with experimental testing and numerical assessment. The main purpose was to discover what the role of the primary residual stress is in fatigue failure, and how the effects of the primary residual stress differ from the effects of the local secondary and tertiary residual stresses.

The results show that the effect of the boundary conditions are clear: specimens welded with high restraint failed faster than the identical, low-restraint specimens. The specimens of low restraint show mean stress dependence to some extent, whereas the high-restraint specimens appear practically as mean stress independent. In general, the fatigue lives were relatively low: the fatigue classes derived from the results are 11–28 % lower than suggested by the design code.

The surface residual stress profiles of the low-restraint specimens are in rather good agreement with the existing literature. The high-restraint specimens, however, show exceptionally high tertiary and secondary stresses: even after releasing the clamp, the tensile residual stress at the toe remains several hundreds of megapascals higher than in the low-restraint case. No notch effect could be recognized to give raise to the primary stresses. Instead, a roughly parallel downwards shift was observed in the residual stress profile after the clamp release.

As a whole, it could not be proved that primary residual stresses alone would have any major effect on the fatigue resistance. Instead, it was noted that changing the welding boundary condition from loose to stiff creates a more serious residual stress state near the toe. This residual stress state is a combination of increased local and global residual stresses, which together have a deteriorating effect on the fatigue strength.

As an additional discovery, it was found that weld peening at a location at a longer distance from the studied weld had a clear effect on the weld residual stress state: HFMI treatment at

30 mm distance from the weld toe brought approximately 100 MPa decrease in tensile residual stress near the toe.

Due to the lack of in-depth residual stress data, the measured residual stresses could not be decomposed into residual stress components (primary, secondary and tertiary). For future research, it is recommended that the through thickness residual stress distributions be either measured with neutron diffractometry, or computed with advanced FEA. Hence, the resultant forces and moments could be determined, and the decomposition would be possible. Hereby, more understanding could be gained on the roles of each residual stress component in the fatigue phenomenon of a welded UHSS joint.

REFERENCES

Berge, S. 1985. Basic Fatigue Properties of Welded Joints. In: Almar-Næss, A. (journalist). 1985. Fatigue Handbook: Offshore Steel Structures. Trondheim: Tapir Forlag. 520 p.

Björk, T., Mettänen, H., Ahola, A., Lindgren, M. & Terva, J. Fatigue Strength Assessment of Duplex and Super-Duplex Stainless Steels by 4R Method. *Welding in the world*, vol. 62:6, pp. 1285–1300.

BS 7910. 2013. Guide to Methods for Assessing the Acceptability of Flaws in Metallic Structures. 3rd edition. The British Standards Institution BSI.

Böhler Welding. 2014. Union X96 Solid wire, low alloyed [Online document]. Published 2014 [Referred 22.1.2020]. Available:
http://www.alruqee.com/Userfiles/Product/TablePdf/19042016000000T_Union%20X%2096_solid%20wire.pdf.

Callister, W. & Rethwisch, D. 2011. *Materials Science and Engineering*. 8th edition. John Wiley & Sons. 885 p.

Dowling, N.E. 2013. *Mechanical Behavior of Materials*. Fourth edition. Harlow: Pearson Education Ltd. 954 p.

EN 1993-1-9. 2005. Eurocode 3: Design of Steel Structures. Part 1–9: Fatigue. Brussels: European Committee for Standardization. 34 p.

Farajian, M. 2013. Welding Residual Stress Behavior under Mechanical Loading. *Welding in the World*, vol. 57, pp. 157–169.

Farajian, M., Nitschke-Pagel, T. & Dilger, K. 2010. Mechanisms of Residual Stress Relaxation and Redistribution in Welded High-Strength Steel Specimens under Mechanical Loading. *Welding in the World*, vol. 54:11-12, pp. 366–374.

Farajian, M., Nitschke-Pagel, T., Wimpory, T.C. & Hofmann, M. 2014. Determination of the Welding Residual Stress Field by Diffraction Methods and Studying its Behavior under Uniaxial and Multiaxial Mechanical Loading. In: Kannengiesser et al. (journalists). 2014. In-situ Studies with Photons, Neutrons and Electrons Scattering II. Switzerland: Springer International Publishing.

Hensel, J., Nitschke-Pagel, T. & Dilger, K. 2016. Effects of Residual Stresses and Compressive mean Stresses on the Fatigue Strength of Longitudinal Fillet-Welded Gussets. *Welding in the world*, vol. 60:2, pp. 267–281.

Hensel, J., Nitschke-Pagel, T. & Dilger, K. 2017. Engineering Model for the Quantitative Consideration of Residual Stresses in Fatigue Design of Welded Components. *Welding in the World*, vol. 61:5, pp. 997–1002.

Hensel, J., Nitschke-Pagel, T., Tchoffo Ngoula, D., Beier, H-T., Tchuindjang, D. & Zerbst, U. 2018. Welding Residual Stresses as Needed for the Prediction of Fatigue Crack Propagation and Fatigue Strength. *Engineering Fracture Mechanics*, vol. 198, pp. 123–141.

Hobbacher, A. 2008. Recommendations for Fatigue Design of Welded Joints and Components. International Institute of Welding, doc. XIII-2151r4-07/XV-1254r4-07.

Kirkhope, K.J., Bell, R., Caron, L., Basu, R.I. & Ma, K.T. 1999. Weld detail fatigue life improvement techniques. Part 1: review. *Marine Structures*, vol. 12:6, pp. 447–474.

Kudryavtsev, I. 1956. The Influence of Internal Stresses on the Fatigue Endurance of Steel. International Conference on Fatigue I. *Mechanical Engineering*, pp. 317–325.

Masubuchi, K. 1980. Analysis of Welded Structures. Residual Stresses, Distortion, and their Consequences. Oxford: Pergamon Press. 642 p.

Masubuchi, K. 1993. Residual Stresses and Distortion. In: *ASM Handbook Vol. 6: Welding, Brazing, and Soldering*. United States: ASM International. pp. 1094–1102.

McClung, R.C. 2007. A Literature Survey on the Stability and Significance of Residual Stresses during Fatigue. *Fatigue & Fracture of Engineering Materials & Structures*, vol. 30:3, pp. 173–205.

Niemi, E. 2003. *Levyrakenteiden suunnittelu*. Helsinki: Teknologiateollisuus Ry. 136 p.

Niemi, E. & Kemppe, J. 1993. *Hitsatun rakenteen suunnittelun perusteet*. Helsinki: Painatuskeskus Oy. 337 p.

Niemi, E., Kilkki, J., Poutiainen, I. & Lihavainen, V-M. 2004. *Väsymättömän hitsausliitoksen suunnittelu*. Fourth edition. Lappeenranta: LTY Digipaino. 121 p.

Nykänen, T. & Björk, T. 2015. Assessment of Fatigue Strength of Steel Butt-welded Joints in As-welded Condition – Alternative Approaches for Curve Fitting and Mean Stress Effect Analysis. *Marine structures*, vol. 44, pp. 288–310.

Nykänen, T. & Björk, T. 2016. A New Proposal for Assessment of the Fatigue Strength of Steel Butt-welded Joints Improved by Peening (HFMI) under Constant Amplitude Tensile Loading. *Fatigue & Fracture of Engineering Materials & Structures*, Vol. 39:5, pp. 566–582.

Paranjpe, S.K. (journalist). 2005. Measurement of residual stress in materials using neutrons. Proceedings of a technical meeting held in Vienna 13–17 October, 2003. International Atomic Energy Agency (IAEA) technical document no. 1457. Vienna: IAEA. 92 p.

Radaj, D. 1992. *Heat Effects of Welding: Temperature Field, Residual Stress, Distortion*. Berlin: Springer Verlag. 348 p.

Sanford, R.J. 2003. *Principles of Fracture Mechanics*. Upper Saddle River: Prentice Hall. 404 p.

Schroepfer, D. & Kannengiesser, T. 2014. Correlating Welding Reaction Stresses and Weld Process conditions for High-strength Steel S960QL. *Welding in the World*, vol. 58:3, pp. 423–432.

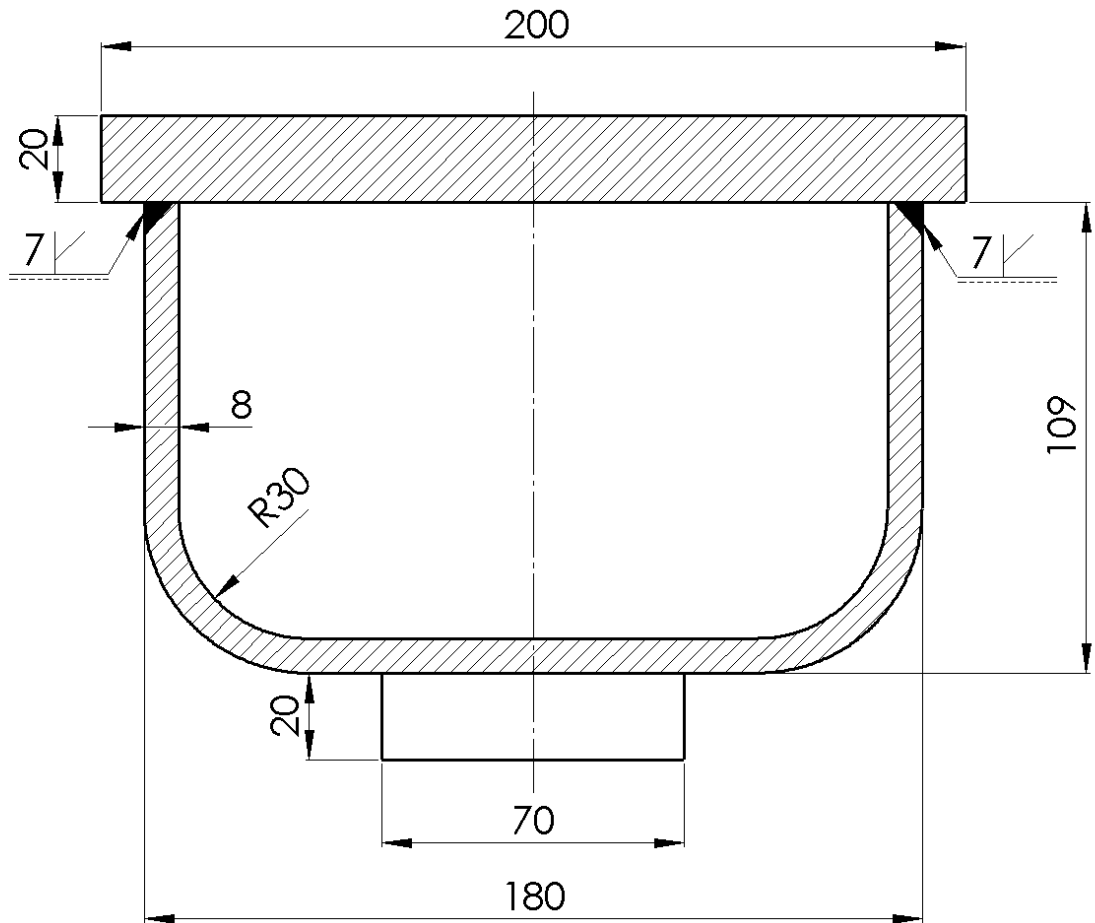
Sonsino, C. 2009a. A Consideration of allowable Equivalent stresses for fatigue Design of Welded Joints According to the Notch Stress Concept with the Reference Radii $r_{ref} = 1.00$ and 0.05 mm. *Welding in the World*, vol. 53:3, pp. R64–R75.

Sonsino, C. 2009b. Effect of residual stresses on the fatigue behavior of welded joints depending on loading conditions and weld geometry. *International Journal of Fatigue*, vol. 31:1, pp. 88–101.

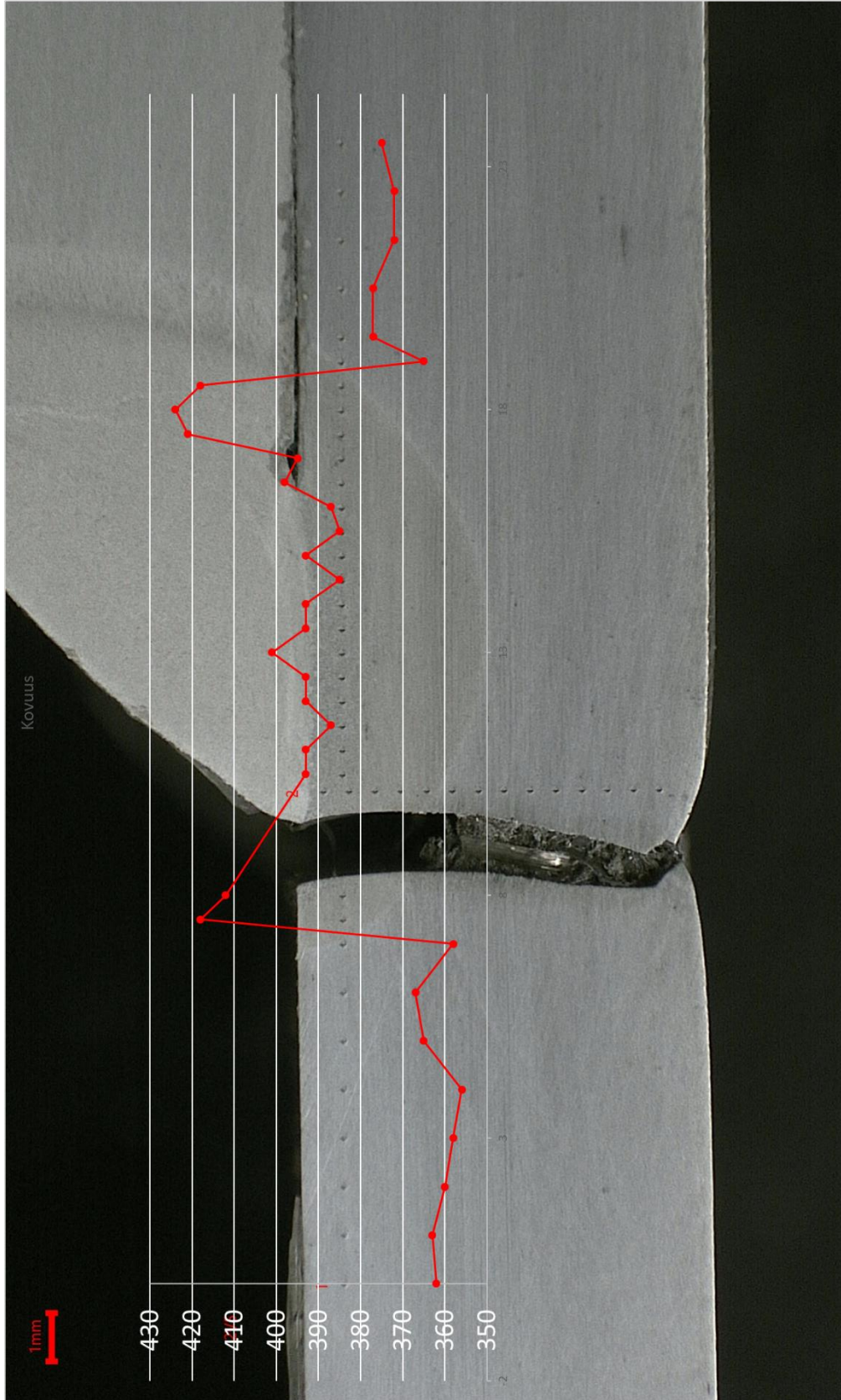
Sonsino, C., Fricke, W., de Bruyne, F., Hoppe, A., Ahmadi, A. & Zhang, G. 2012. Notch Stress Concepts for the Fatigue Assessment of Welded Joints – Background and Applications. *International Journal of Fatigue*, vol. 34:1, pp. 2–16.

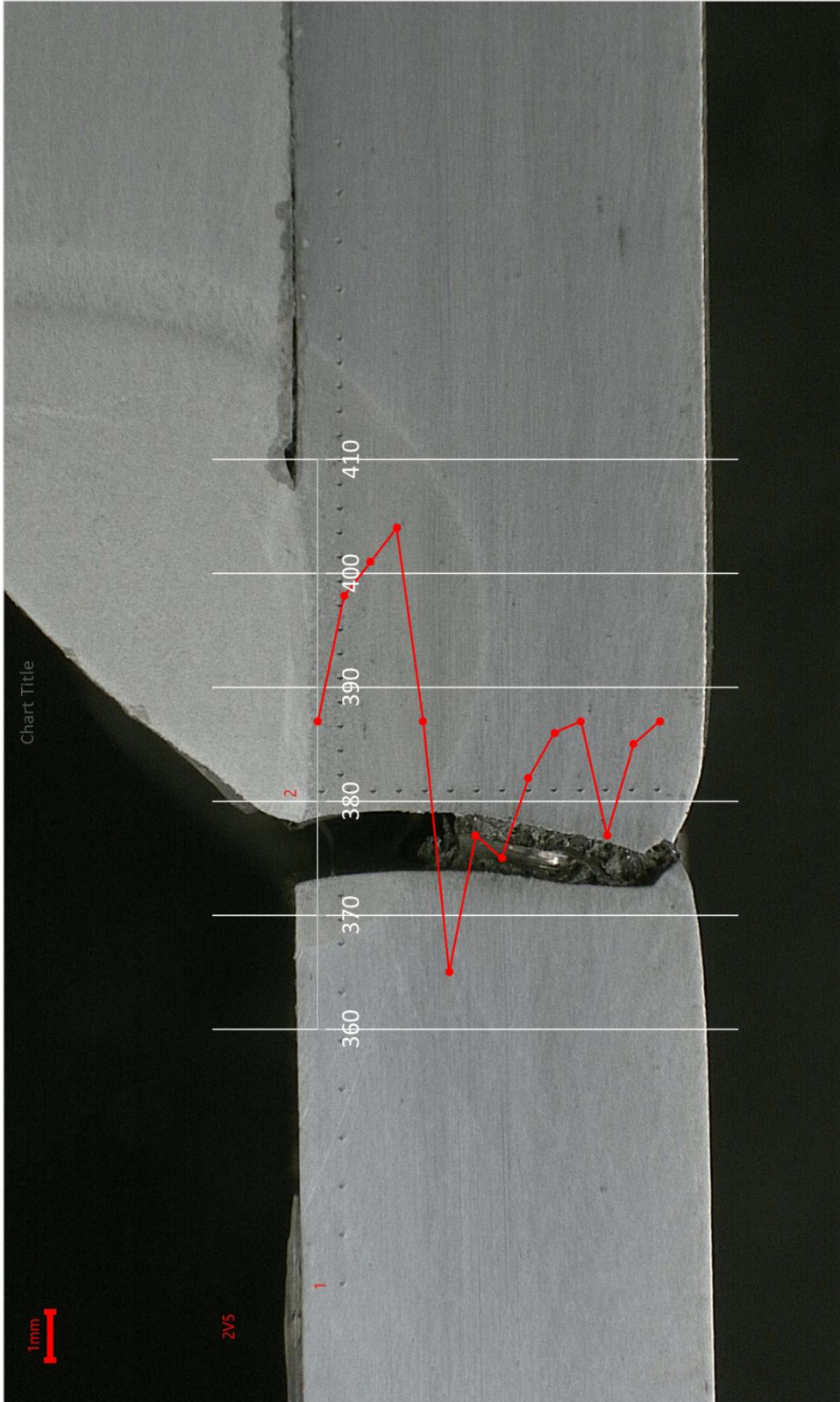
SSAB. 2020. Strenx® 1100 Plus. [web document]. [Referred 5.3.2020]. Available: <https://www.ssab.com/products/brands/strenx/products/strenx-1100-plus>

Cross section of batch 3 specimen.



Vickers hardness distributions of weld area.





Strain alterations in batch 3 specimens during HFMI treatment.

